
RELAXING RESTRICTIONS AT THE PACE OF VACCINATION INCREASES FREEDOM AND GUARDS AGAINST FURTHER COVID-19 WAVES

Simon Bauer^{1,¶}, Sebastian Contreras^{1,2,¶}, Jonas Dehning¹, Matthias Linden^{1,3}, Emil Iftekhar¹,
Sebastian B. Mohr¹, Alvaro Olivera-Nappa², and Viola Priesemann^{1,4*}

¹Max Planck Institute for Dynamics and Self-Organization, Am Faßberg 17, 37077 Göttingen, Germany.

²Centre for Biotechnology and Bioengineering, Universidad de Chile, Beauchef 851, 8370456 Santiago, Chile.

³Institute for Theoretical Physics, Leibniz University, 30167 Hannover.

⁴Institute for the Dynamics of Complex Systems, University of Göttingen, Friedrich-Hund-Platz 1, 37077 Göttingen, Germany.

¶ These authors contributed equally

Abstract

Mass vaccination offers a promising exit strategy for the COVID-19 pandemic. However, as vaccination progresses, demands to lift restrictions increase, despite most of the population remaining susceptible. Using our age-stratified SEIRD-ICU compartmental model and curated epidemiological and vaccination data, we quantified the rate (relative to vaccination progress) at which countries can lift non-pharmaceutical interventions without overwhelming their healthcare systems. We analyzed scenarios ranging from immediately lifting restrictions (accepting high mortality and morbidity) to reducing case numbers to a level where test-trace-and-isolate (TTI) programs efficiently compensate for local spreading events. In general, the age-dependent vaccination roll-out implies a transient decrease of more than ten years in the average age of ICU patients and deceased. The pace of vaccination determines the speed of lifting restrictions; Taking the European Union (EU) as an example case, all considered scenarios allow for steadily increasing contacts starting in May 2021 and relaxing most restrictions by autumn 2021. Throughout summer 2021, only mild contact restrictions will remain necessary. However, only high vaccine uptake can prevent further severe waves. Across EU countries, seroprevalence impacts the long-term success of vaccination campaigns more strongly than age demographics. In addition, we highlight the need for preventive measures to reduce contagion in school settings throughout the year 2021, where children might be drivers of contagion because of them remaining susceptible. Strategies that maintain low case numbers, instead of high ones, reduce infections and deaths by factors of eleven and five, respectively. In general, policies with low case numbers significantly benefit from

*viola.priesemann@ds.mpg.de

vaccination, as the overall reduction in susceptibility will further diminish viral spread. Keeping case numbers low is the safest long-term strategy because it considerably reduces mortality and morbidity and offers better preparedness against emerging escape or more contagious virus variants while still allowing for higher contact numbers ("freedom") with progressing vaccinations.

Author summary

In this work, we quantify the rate at which non-pharmaceutical interventions can be lifted as COVID-19 vaccination campaigns progress. With the constraint of not exceeding ICU capacity, there exists only a relatively narrow range of plausible scenarios. We selected different scenarios ranging from the immediate release of restrictions to more conservative approaches aiming at low case numbers. In all considered scenarios, the increasing overall immunity (due to vaccination or post-infection) will allow for a steady increase in contacts. However, deaths and total cases (potentially leading to *long covid*) are only minimized when aiming for low case numbers, and restrictions are lifted at the pace of vaccination. These qualitative results are general. Taking EU countries as quantitative examples, we observe larger differences only in the long-term perspectives, mainly due to varying seroprevalence and vaccine uptake. Thus, the recommendation is to keep case numbers as low as possible to facilitate test-trace-and-isolate programs, reduce mortality and morbidity, and offer better preparedness against emerging variants, potentially escaping immune responses. Keeping moderate preventive measures in place (such as improved hygiene, use of face masks, and moderate contact reduction) is highly recommended will further facilitate control.

Introduction

The rising availability of effective vaccines against SARS-CoV-2 promises the lifting of restrictions, thereby relieving the social and economic burden caused by the COVID-19 pandemic. However, it is unclear how fast the restrictions can be lifted without risking another wave of infections; we need a promising long-term vaccination strategy [1]. Nevertheless, a successful approach has to take into account several challenges; vaccination logistics and vaccine allocation requires a couple of months [2–4], vaccine eligibility depends on age and eventually serostatus [5], vaccine acceptance may vary across populations [6], and more contagious [7] and escape variants of SARS-CoV-2 that can evade existing immunity [8,9] may emerge, thus posing a persistent risk. Last but not least, disease mitigation is determined by how well vaccines block infection, and thus prevent the propagation of SARS-CoV-2 [3,4], the time to develop effective antibody titers after vaccination, and their efficacy against severe symptoms. All these parameters will greatly determine the design of an optimal strategy for the transition from epidemicity to endemicity [10].

To bridge the time until a significant fraction of the population is vaccinated, a sustainable public health strategy has to combine vaccination with non-pharmaceutical interventions (NPIs). Otherwise it risks further waves and, consequently, high morbidity and excess mortality. However, the overall compliance with NPIs worldwide has on average decreased due to a “pandemic-policy fatigue” [11]. Therefore, the second wave has been more challenging to tame [12] although NPIs, in principle, can be highly effective, as seen in the first wave [13,14]. After vaccinating the most vulnerable age groups, the urge and social pressure to lift restrictions will increase. However, given the wide distribution of fatalities over age groups and the putative incomplete protection of vaccines against severe symptoms and against transmission, NPIs cannot be lifted

entirely or immediately. With our study, we want to outline at which pace restrictions can be lifted as the vaccine roll-out progresses.

Public-health policies in a pandemic have to find a delicate ethical balance between reducing the viral spread and restricting individual freedom and economic activities. However, the interest of health on the one hand and society and economy on the other hand are not always contradictory. For the COVID-19 pandemic, all these aspects clearly profit from low case numbers [15–17], i.e., an incidence where test-trace-and-isolate (TTI) programs can efficiently compensate for local spreading events. The challenge is to reach low case numbers and maintain them [18, 19]. Especially with the progress of vaccination, restrictions should be lifted when the threat to public health is reduced. However, the apparent trade-off between public health interest and freedom is not always linear and straightforward. Taking into account that low case numbers facilitate TTI strategies (i.e. health authorities can concentrate on remaining infection chains and stop them quickly) [18–20], an optimal strategy with a low public health burden *and* large freedom may exist and be complementary to vaccination.

Here, we quantitatively study how the planned vaccine roll-out in the European Union (EU), together with the cumulative post-infection immunity (seroprevalence), progressively allows for lifting restrictions. In particular, we study how precisely the number of contacts can be increased without rendering disease spread uncontrolled over the year 2021. Our study builds on carefully curated epidemiological and contact network data from Germany, France, the UK, and other European countries. Thereby, our work can serve as a blueprint for an opening strategy.

Analytical framework

Our analytical framework builds on our deterministic, age-stratified, SEIRD-ICU compartmental model, modified to incorporate vaccination through delay differential equations (schematized in Fig. 6). It includes compartments for a 2-dose staged vaccine roll-out, immunization delays, intensive care unit (ICU)-hospitalized, and deceased individuals. A central parameter for our model is the gross reproduction number R_t . It is essentially the time-varying effective reproduction number without considering the effects of immunity nor of TTI. That number depends (among several factors) on i) the absolute number of contacts per individual, and ii) the probability of being infected given a contact. In other words, R_t is defined as the average number of contacts an infected individual has that would lead to an offspring infection in a fully susceptible population. Therefore, an increase in R_t implies an increase in contact frequency or the probability of transmission per contact, e.g., due to less mask-wearing. The core idea is that increasing immunity levels among the population (post-infection or due to vaccination) allows for a higher average number of potentially contagious contacts and, thus, freedom (quantified by R_t), given the same level of new infections or ICU occupancy. Hence, with immunization progress reducing the susceptible fraction of the population, R_t can be dynamically increased while maintaining control over the pandemic, i.e., while keeping the effective reproduction number below one (Fig. 1 A).

To adapt the gross reproduction number R_t such that a specific strategy is followed (e.g. staying below TTI or ICU capacity), we include an automatic, proportional-derivative (PD) control system [21]. This control system allows for steady growth in R_t as long as it does not lead to overflowing ICUs (or surpassing the TTI capacity). However, when risking surpassing the ICU capacity, restrictions might be tightened again. In that way, we approximate the feedback-loop between political decisions, people’s behavior, reported case numbers, and ICU occupancy.

The basic reproduction number is set to $R_0 = 4.5$, reflecting the dominance of the B.1.1.7 variant [3, 7]. We further assume that the reproduction number can be decreased to about 3.5 by hygiene measures, face masks, and mild social distancing. This number is informed by the estimates of Sharma et al. [22], who estimate the combined effectiveness of mask wearing, limiting gatherings to at most 10 people and closing night clubs to a reduction of about 20–40%, thus leading to a reproduction number between 2.7 and 3.6. We use a conservative estimate, as this is only an exemplary set of restrictions. Therefore, we restrict R_t in general not to exceed 3.5 (Fig. 1 C). All other parameters (and their references) are listed in Table 5.

Efficient TTI contributes to reducing the effective reproduction number. Hence, it increases the average number of contacts (i.e., R_t) that people may have under the condition that case numbers remain stable (Fig. 1A) [18]. This effect is particularly strong at low case numbers, where the health authorities can concentrate on tracing every case efficiently [19]. Here, we approximate the effect of TTI on R_t semi-analytically to achieve an efficient implementation (see Methods).

For vaccination, we use as default parameters an average vaccine efficacy of 90% protection against severe illness [23] and of 75% protection against infection [24]. We further assume that vaccinated individuals with a breakthrough infection carry a lower viral load and thus are 50% less infectious [25] than unvaccinated infected individuals. We assume an average vaccine uptake of 80% [26] that varies across age (see Table 2), and an age-prioritized vaccine delivery as described in the Methods section. In detail, most of the vaccines are distributed first to the age group 80+, then 70+, 60+, and then to anyone of age 16+. A small fraction of the weekly available vaccines is distributed randomly (e.g. because of profession). After everyone got a vaccine offer roughly by the end of August, we assume no further vaccination (see Fig. 2L). The daily amount of vaccine doses per million is derived from German government projections, but is expected to be similar across the EU. For the course of the disease, the age-dependent fraction of non-vaccinated, infected individuals requiring intensive care is estimated from German hospitalization data, using the infection-fatality-ratio (IFR) reported in [27] (see Table 1 and Methods).

In our default scenario we use a contact structure between age groups as measured during pre-pandemic times [28]. However, we halve the infection probability in the 0–19 year age group to account for reduced in-person classes and better ventilation and systematic random screening in school settings using rapid COVID-19 tests. Under these assumptions, the infection probability among the 0–19 age group is similar to the one among the 20–39 and 40–69 age groups (Fig. 7). We start our simulations at the beginning of March 2021, with an incidence of 200 daily infections per million, two daily deaths per million, an ICU occupancy of 30 patients per million, a seroprevalence of 10%, and about 4% of the population already vaccinated. This is comparable to German data (assuming a case under-reporting factor of 2, which had been measured during the first wave in Germany [29]) and typical for EU countries at the beginning of March 2021 (further details in the Methods section). We furthermore explore the impact of important differences between EU countries, namely the seroprevalance by the start of the vaccination program, demographics, and vaccine uptake exemplary for Finland, Italy and the Czech Republic in addition to the default German parameters.

Results

Aiming for low case numbers has the best long-term outcome

We first present the two extreme scenarios: case numbers quickly rise so that the ICU capacity limit is approached (scenario 1), or case numbers quickly decline below the TTI capacity limit (scenario 5; Fig.

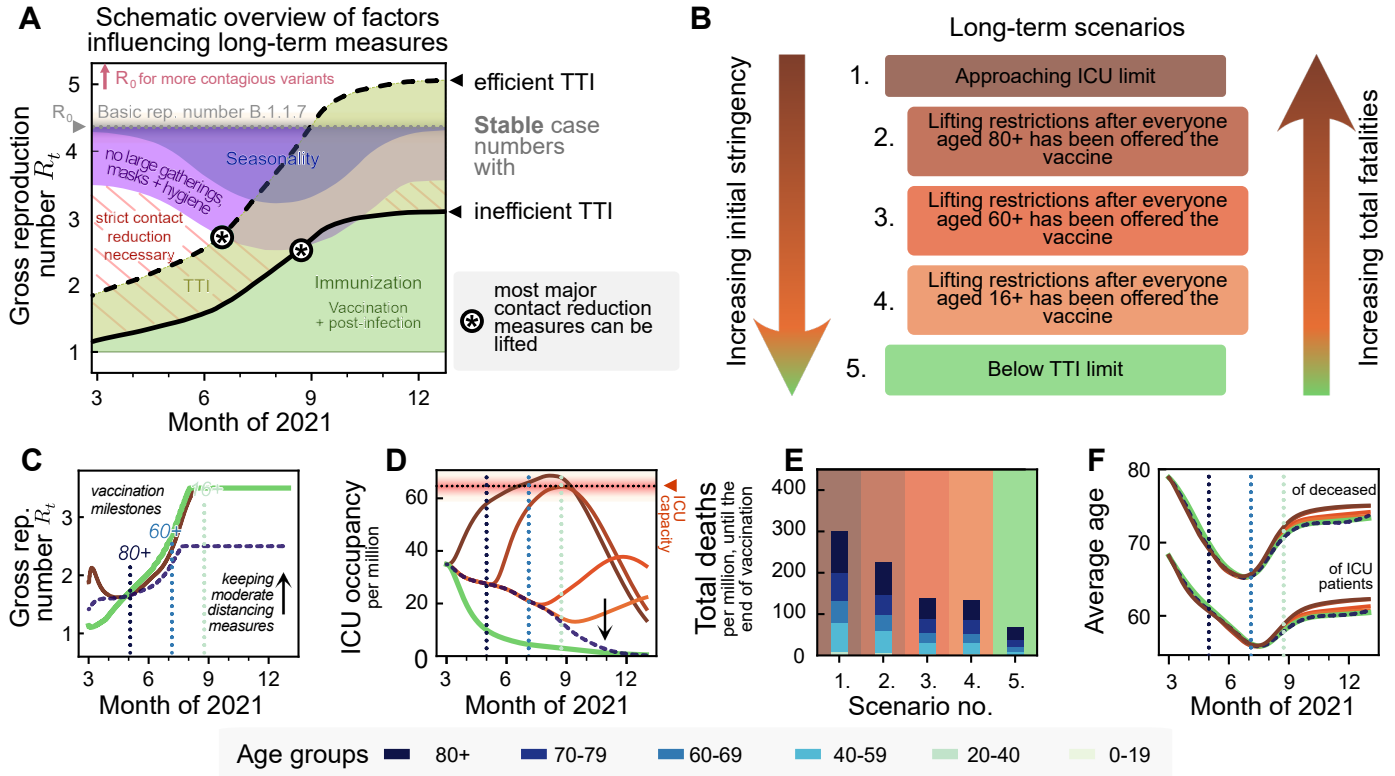


Figure 1: **With progressing vaccination in the European Union, a slow but steady increase in freedom will be possible. However, premature lifting of NPIs considerably increases the total fatalities without a major reduction in restrictions in the middle term.** **A:** A schematic outlook into the effect of vaccination on societal freedom. Freedom is quantified by the maximum time-varying gross reproduction number (R_t) allowed to sustain stable case numbers. As R_t does not consider the immunized population, gross reproduction numbers above one are possible without rendering the system unstable. A complete return to pre-pandemic behavior would be achieved when R_t reaches the value of the basic reproduction number R_0 (or possibly at a lower value due to seasonality effects during summer, purple-blue shaded area). The thick full and dashed lines indicate the gross reproduction number R_t allowed to sustain stable case numbers if test-trace-isolate (TTI) programs are inefficient and efficient, respectively, which depends on the case numbers level. Increased population immunity (green) is expected to allow for lifting the most strict contact reduction measures while only keeping mild NPIs (purple) during summer 2021 in the northern hemisphere. Note that seasonality is not explicitly modeled in this work. See Supplementary Fig S4 for an extended version including the year 2020. **B:** We explore five different scenarios for lifting restrictions in the EU, in light of the EU-wide vaccination programs. We sort them according to the initial stringency that they require and the total fatalities that they may cause. One extreme (scenario 1) offers immediate (but still comparably little) freedom by approaching ICU-capacity limits quickly. The other extreme (scenario 5) uses a strong initial reduction in contacts to allow long-term control at low case numbers. Finally, the intermediate scenarios initially maintain moderate case numbers and lift restrictions at different points in the vaccination program. **C:** All extreme strategies allow for a steady noticeable increase in contacts in the coming months (cf. panel A), but vary greatly in the (D) ICU-occupancy profiles and (E) total fatalities. **F:** Independent on the strategy, we expect a transient but pronounced decrease in the average age of ICU patients and deceased over the summer.

Fig. 2). We set the ICU capacity limit at 65 patients/million, reflecting the maximal occupancy and improved treatments during the second wave in Germany [30] and use German demographics. The incidence (daily

Table 1: **Age-dependent infection-fatality-ratio (IFR), probability of requiring intensive care due to the infection (ICU probability) and ICU fatality ratio (ICU-FR).** The IFR is defined as the probability of an infected individual dying, whereas the ICU-FR is defined as the probability of an infected individual dying while receiving intensive care.

Age	IFR ([27])	ICU probability	ICU-FR	Avg. ICU time (days)
0-19	0.000 02	0.000 14	0.0278	5
20-39	0.000 22	0.002 03	0.0389	5
40-59	0.001 94	0.012 17	0.0678	11
60-69	0.007 39	0.040 31	0.1046	11
70-79	0.023 88	0.054 35	0.1778	9
>80	0.082 92	0.071 63	0.4946	6
Average	0.009 57	0.020 67	0.0969	9

new cases) limit up to which TTI is fully efficient is set to 20 daily infections per million [15], but depends strongly on the gross reproduction number, as described in Methods.

The first scenario (‘approaching ICU limit’, Fig. 2A–D) maximizes the initial freedom individuals might have (quantified as the allowed gross reproduction number R_t). However, the gained freedom is only transient as, once ICUs approach their capacity limit, restrictions need to be tightened (Fig. 2 J,K). Additionally, stabilization at high case numbers leads to many preventable fatalities, especially in light of likely temporary overflows of the ICU capacity due to the hard-to-control nature of high case numbers.

The fifth scenario (‘below TTI limit’, Fig. 2E–F) requires maintaining stronger restrictions for about two months to lower case numbers below the TTI capacity. Afterward, the progress of the vaccination allows for a steady increase in R_t while keeping case numbers low, enabling TTI to contribute to the containment effectively. From May 2021 on, this fifth scenario would allow for slightly more freedom, i.e., a higher R_t , than the first scenario (Fig. 1C). Furthermore, this scenario reduces morbidity and mortality: Deaths until the of the vaccination period (end of August) are reduced by a factor of five, total infections even by a factor of eleven. Due to the prioritization of the elderly in vaccination, the average age of ICU patients and fatalities drops by roughly 12 and 15 years, respectively, independently of the choice of scenarios (Fig. 2 I). Overall, the low-case-number scenario thus allows for a very similar increase in freedom over the whole time frame (quantified as the increase in R_t) and implies about fives times fewer deaths by the end of the vaccination program compared to the first scenario with high case numbers (Fig. 2 K).

The vaccine uptake has little influence on the number of deaths and total cases during the vaccination period (Fig. 2 J,K), mainly because restrictions are quickly enacted when reaching the ICU capacity. However, uptake becomes a crucial parameter; It controls the pandemic progression after completing the vaccine roll-out as it determines the residual susceptibility of the population (cf. Fig. 4). With insufficient vaccination uptake, a novel wave will follow as soon as restrictions are lifted [3].

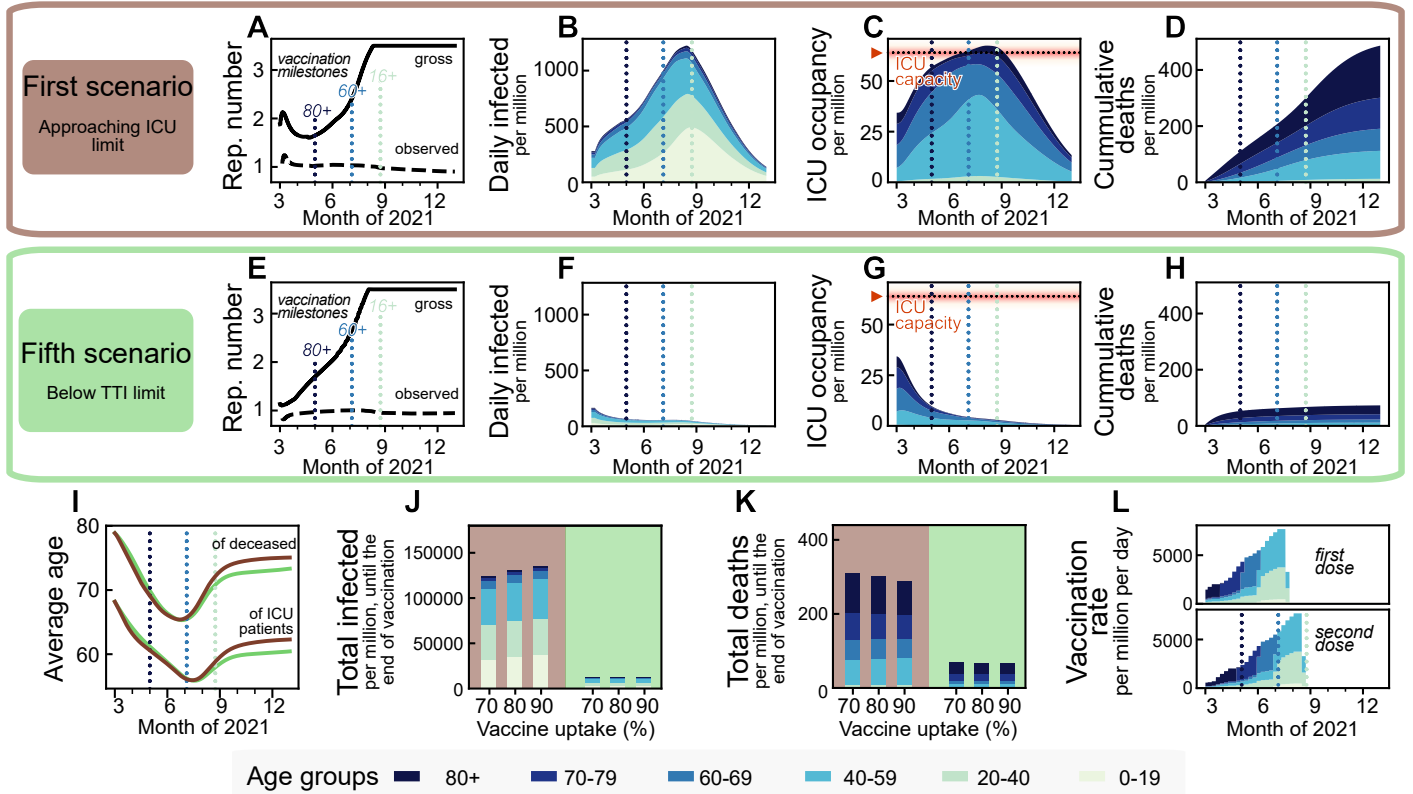


Figure 2: **Maintaining low case numbers during vaccine roll-out reduces the number of ICU patients and deaths by about a factor five compared to quickly approaching the ICU limit while hardly requiring stronger restrictions.** Aiming to maximize ICU occupancy (A–D) allows for a slight increase of the allowed gross reproduction number R_t early on, whereas lowering case numbers below the TTI capacity limit (E–H) requires comparatively stronger initial restrictions. Afterwards, the vaccination progress allows for a similar increase in freedom (quantified by increments in R_t) for both strategies, starting approximately in May 2021. B–D, F–H: These two strategies lead to a completely different evolution of case numbers, ICU occupancy, and cumulative deaths, but differ only marginally in the evolution of the average age of deceased and ICU patients (I), as the latter is rather an effect of the age-prioritized vaccination than of a particular strategy. J, K: The total number of cases until the end of the vaccination period (of the 80% uptake scenario, i.e., end of August, the rightmost dotted light blue line in sub-panels A–H) differ by a factor of eleven between the two strategies, and the total deaths by a factor of five. Vaccine uptake (i.e., the fraction of the eligible, 16+, population that gets vaccinated) has a minor impact on these numbers until the end of the vaccine roll-out but determines whether a wave would follow afterward (see Fig. 4). L: Assumed vaccination rate as projected for Germany, which is expected to be similar across the European Union. For a full display of the time-evolution of the compartments for different uptakes see Supplementary Figs S6–S8.

Maintaining low case numbers at least until vulnerable groups are vaccinated is necessary to prevent a severe further wave

Between the two extreme scenarios 1 and 5, which respectively allow maximal or minimal initial freedom, we explore three alternative scenarios, where the vaccination progress and the slow restriction lifting roughly balance out (Figs. 3, 1 B). These scenarios assume approximately constant case numbers and then a swift lifting of most of the remaining restrictions within a month after three different vaccination milestones: when the age group 80+ has been vaccinated (scenario 2, Fig. 3 A–D), when the age groups 60+ has been

vaccinated (scenario 3, Fig. 3 E–H) and when the entire adult population (16+) has been vaccinated (scenario 4, Fig. 3 I–L).

The relative freedom gained by lifting restrictions early in the vaccination timeline (scenario 2) hardly differs from the freedom gained from the other two scenarios (Fig. 3 M), as since new contact restrictions need to take place once reaching the ICU capacity limit, and the initial freedom is partly lost. Significantly, lifting restrictions later reduces the number of infections and deaths by more than 50% and 35% respectively if case numbers have been kept at a moderate level (250 daily infections per million) and by more than 85% and 65%, respectively if case numbers have been kept at a low level (50 per million) beforehand (Fig. 3 N,O). Lifting restrictions entirely after either offering vaccination to everyone aged 60+ or everyone aged 16+ only changes the total fatalities by a small amount, mainly because the vaccination pace is planned to be quite fast by then, and the 60+ age brackets make up the bulk of the highest-risk groups. Hence, a potential subsequent wave only unfolds after the end of the planned vaccination campaign (Fig. 3 F-H). Thus, with the current vaccination plan, it is recommended to keep case numbers at moderate or low levels, at least until the population at risk and people of age 60+ have been vaccinated.

If maintaining low or intermediate case numbers in the initial phase, vaccination starts to decrease the ICU occupancy considerably in May 2021 (Fig. 3 G,K). However, This decrease in ICU occupancy must not be mistaken for a generally stable situation. As soon as restrictions are relaxed too quickly, ICU occupancy surges again (Fig. 3 C,G,H), without any relevant gain in freedom for the total population. Nonetheless, the progress in vaccination will, in any case, allow lifting restrictions gradually.

The long-term success of the vaccination campaign strongly depends on vaccine uptake and vaccine efficacy

The vaccination campaign’s long-term success will depend on both people’s vaccine uptake (see Table 2) and the efficacy of the vaccine against those variants of SARS-CoV-2 prevalent at the time of writing of this paper. A vaccine’s efficacy has two contributions: first, vaccinated individuals become less likely to develop severe symptoms and require intensive care [31–33] (vaccine efficacy, κ). Second, a fraction η of vaccinated individuals gains sterilizing immunity, i.e., is completely protected against infections and does not contribute to viral spread at all [24,34]. We also assume that breakthrough infections among vaccinated individuals would bear lower viral loads, thus exhibit reduced transmissibility [25] (reduced viral load, σ). However, the possibly reduced effectiveness of vaccines against current variants of concern (VOCs), e.g., B.1.351 and P.1 [32,35,36], and potential future VOCs render long-term scenarios about the success of vaccination uncertain.

Therefore, we explore different parameters of vaccine uptake and effectiveness. We quantify the success, or rather the lack of success of the vaccination campaign by the duration of the period where ICUs function near capacity limit, until population immunity is reached. Two different scenarios are considered upon finishing the vaccination campaign: in the first scenario, most restrictions are lifted, like in the previous scenarios (Fig. 4 B). In the second, restrictions are only lifted partially, to a one third lower gross reproduction number ($R_t = 2.5$) (Fig. 4 C). This second scenario presents the long-term maintenance of moderate social distancing measures, including the restriction of large gatherings to smaller than 100 people, encouraging home-office, enabling effective test-trace-and-isolate (TTI) programs at very low case numbers, and supporting hygiene measures and face mask usage. Fig 4B,C indicates how long ICUs are expected to be full in both scenarios,

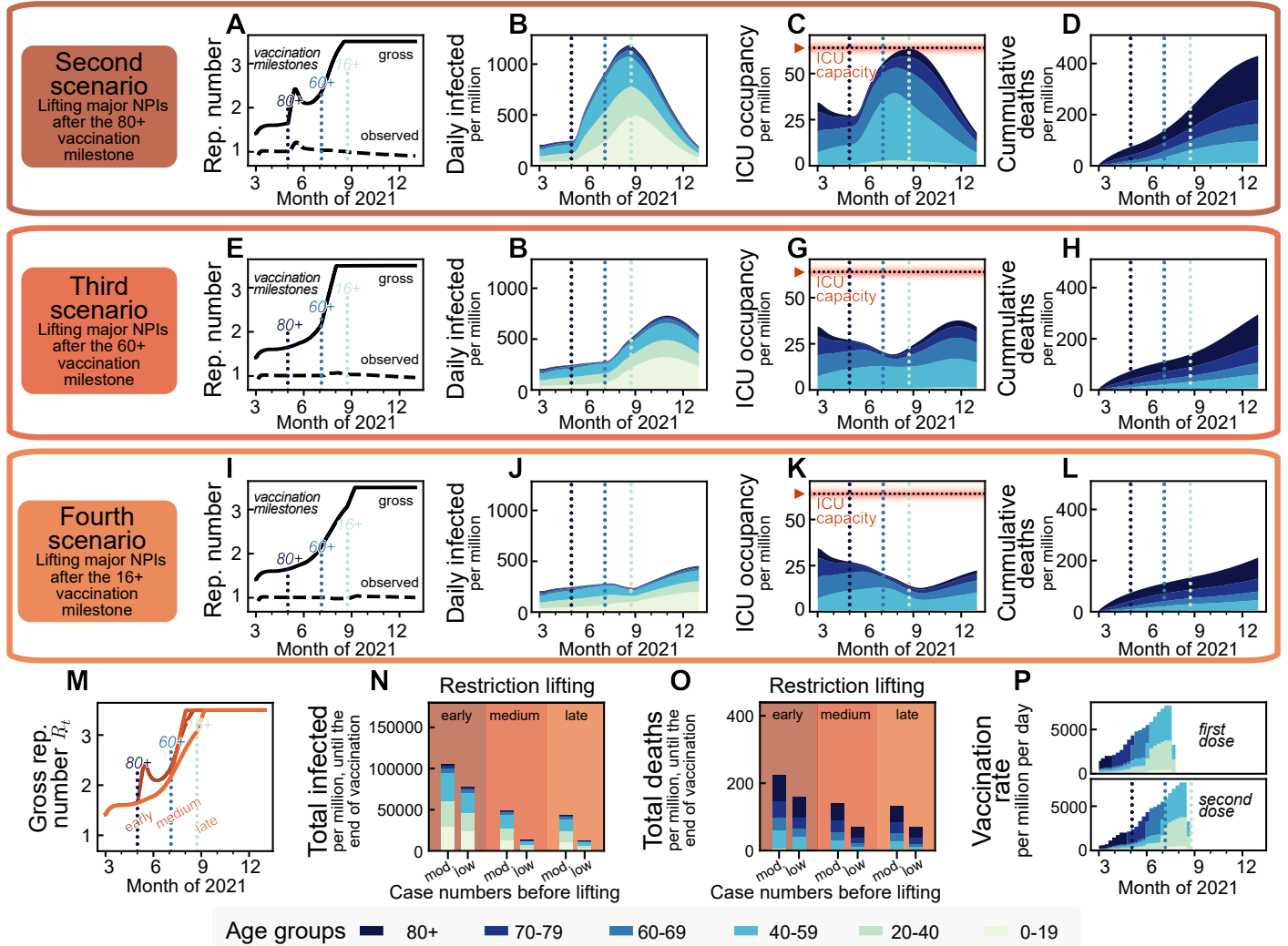


Figure 3: **Vaccination offers a steady return to normality until the end of summer 2021 in the northern hemisphere, no matter whether a transient easing of restrictions is allowed earlier or later (second and fourth scenario, respectively). However, lifting restrictions later reduces fatalities by more than 35%.** We assume that the vaccine immunization progress is balanced out by a slow lifting of restrictions, keeping case numbers at a moderate level (≤ 250 daily new cases per million people). We simulated lifting all restrictions within a month starting from different time points: when (A–D) the 80+ age group, (E–H) the 60+ age group or (I–L) everyone 16+ has been offered vaccination. Restriction lifting leads to a new surge of cases in all scenarios. New restrictions are put in place if ICUs would otherwise collapse. **M:** Lifting all restrictions too early increases the individual freedom only temporarily before new restrictions have to be put in place to avoid overwhelming ICUs. Overall, trying to lift restrictions earlier has a small influence on the additional increase in the allowed gross reproduction number R_t . **N,O:** Relaxing major restrictions only medium-late or late reduces fatalities by more than 35% and infections by more than 50%. Fatalities and infections can be cut by an additional factor of more than two when aiming for a *low* (50 per million) instead of *moderate* (250 per million) level of daily infections before major relaxations. **P:** Assumed daily vaccination rates, same as in Figure 2.

and for different parameters of vaccine efficacy (which may account for the emergence of vaccine escape variants).

The primary determinant for the success of vaccination programs after lifting most restrictions is the vaccine uptake among the population aged 20+; only with a high vaccine uptake ($> 90\%$) we can avoid a novel wave of full ICUs (default parameters as in scenario 3; Fig. 4B, $\kappa = 90\%$, $\eta = 75\%$). However, if vaccine uptake was lower or vaccines prove to be less effective against prevalent or new variants, lifting most restrictions would imply that ICUs will work at the capacity limit for months.

In contrast, maintaining moderate social distancing measures (Fig. 4C) may prevent a wave after completing the vaccine roll-out. This strategy can also compensate for a low vaccine uptake, requiring only about 55% uptake to avoid surpassing ICU capacity for our default parameters. Nonetheless, any increase in vaccine uptake lowers intensive care numbers, increases freedom, and most importantly, provides better protection in case of the emergence of escape variants, as this would involve an effective reduction of vaccine efficacy (dashed lines). A full exploration of vaccine efficacy parameter combinations and different contact structures is presented in Supplementary Fig S2.

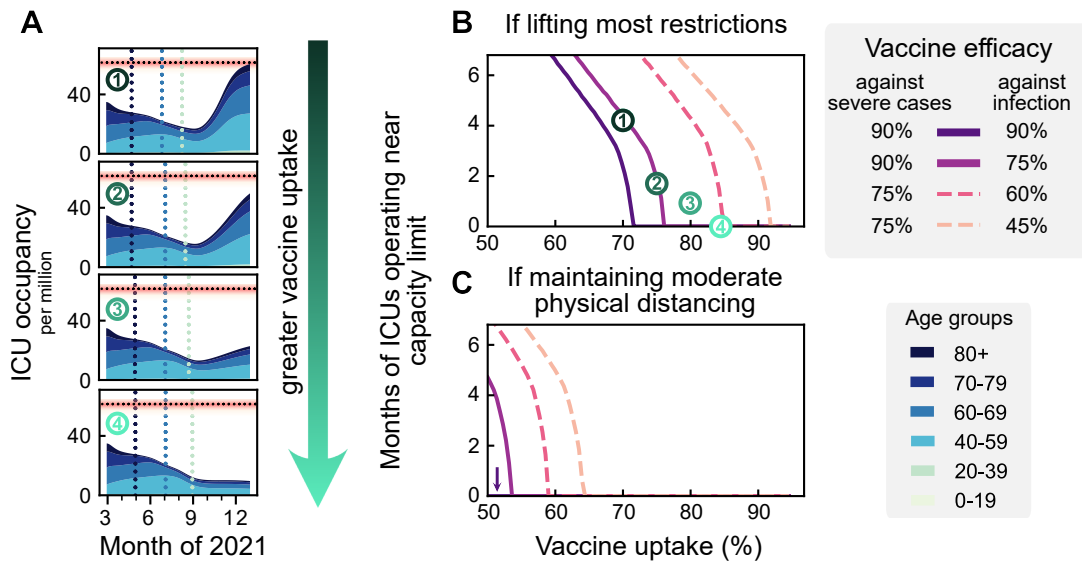


Figure 4: **A high vaccine uptake ($> 90\%$ or higher among the eligible population) is crucial to prevent a wave when lifting restrictions after completing vaccination campaigns.** **A:** We assume that infections are kept stable at 250 daily infections until all age groups have been vaccinated. Then restrictions are lifted, leading to a wave if the vaccine uptake has not been high enough (top three plots). **B:** The duration of the wave (measured by the total time that ICUs function close to their capacity limit) depends on vaccine uptake and vaccine efficacy. We explore the dependency on the efficacy both for preventing severe cases (full versus dashed lines) and preventing infection (shades of purple). The dashed lines might correspond to vaccine efficacy in the event of the emergence of escape variants of SARS-CoV-2. **C:** If some NPIs remain in place (such that the gross reproduction number stays at $R_t = 2.5$), ICUs will not overflow even if the protection against infection is only around 60%. See Supplementary Fig S2 for all possible combinations of vaccine efficacies, also in the event of different contact structures.

Heterogeneity among countries on an EU-wide level will affect the probability and strength of a new wave after completing vaccination campaigns. We chose some exemplary European countries to investigate how our results depend on age demographics, contact structure, and the degree of initial post-infection immunization (seroprevalence). We obtained the seroprevalence in the different countries by scaling the German 10% seroprevalence with the relative differences in cumulative reported case numbers between Germany and the other countries, i.e., we assume the under-reporting factor to be roughly the same across the chosen countries.

All other parameters are left unchanged. Specifically, we leave the capacities of the health systems at the estimated values for Germany, as lacking TTI data and varying definitions of ICU treatment make any comparison difficult. We repeated the analysis presented above (Fig. 4) for Finland, Italy and the Czech Republic (see Fig. 5 A–D). Germany, Finland, and Italy would need a similarly high vaccine uptake in the population to prevent another severe wave. In the Czech Republic, a much smaller uptake is sufficient. The largest deviations in the necessary vaccine uptake are due to the initial seroprevalence, which we estimate to range from 5% in Finland to 30% in the Czech Republic. In contrast, the differences in age demographics and contact structures only have a minor effect on the dynamics (see also Supplementary Fig S1).

If no further measures remain in place to reduce the potential contagious contacts in school settings, the young age group (0–19 years) will drive infections after completing the vaccination program as they remain mostly unvaccinated. The combination of intense contacts and high susceptibility among school-aged children considerably increase the vaccine uptake required in the adult population to restrain a further wave (Fig. 5 E–H). High seroprevalence, also in this age group, reduces the severity of this effect for the Czech Republic (Fig. 5 H).

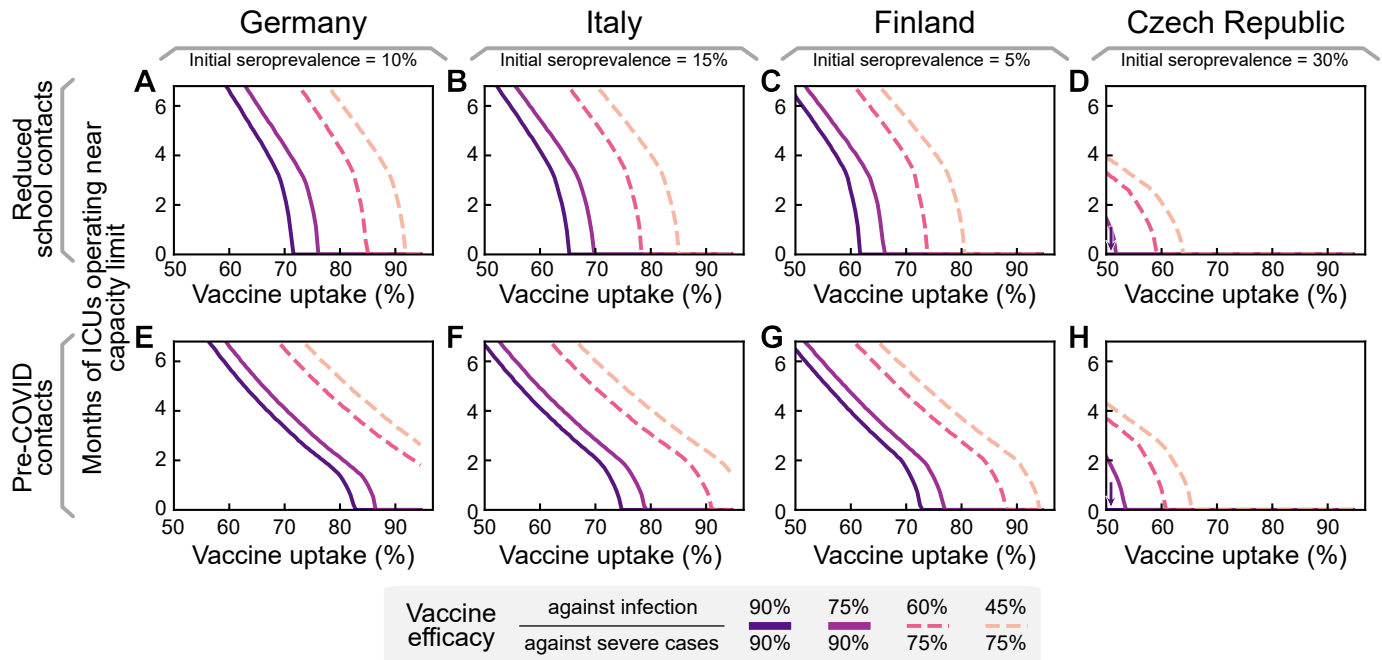


Figure 5: **Seroprevalence and different demographics across EU countries determine the vaccine uptake required for population immunity.** As in Fig. 4 B, we assume that case numbers are stable at 250 daily infections per million per day until the end of vaccination, when most restrictions are lifted (such that the gross reproduction number goes up to 3.5). We vary the initial seroprevalence and age demographics and contact structures to represent German, Italian, Finnish, and Czech data. **A–D:** Projected ICU occupancy in a subsequent wave depending on vaccine uptake, assuming reduced transmission risk in schools but otherwise default pre-pandemic contact structures. **E–H:** Projected ICU occupancy depending on vaccine uptake, assuming default pre-pandemic contact structures everywhere (including schools). See Supplementary Fig S3 for a more comprehensive exploration of combinations of vaccine efficacies.

Discussion

Our results demonstrate that the pace of vaccination first and foremost determines the expected gain in freedom (i.e., lifting of restrictions) during and after completion of the COVID-19 vaccination programs. Any premature lifting of restrictions risks another wave with high COVID-19 incidence and full ICUs. Moreover, the increase in freedom gained by these premature strategies is only transient because once ICU capacity is reached again, restrictions would have to be reinstated. Simultaneously, these early relaxations significantly increase morbidity and mortality rates, as a fraction of the population has not yet been vaccinated and thus remains susceptible. In contrast, maintaining low case numbers avoids another wave, and *still* allows to lift restrictions steadily and at a similar pace as with high case numbers. Despite this qualitative behavior being general, the precise quantitative results depend on several parameters and assumptions, which we discuss in the following.

The specific time evolution of the lifting of restrictions is dependent on the progress of the vaccination program. Therefore, a steady lifting of restrictions may start in May 2021, when the vaccination rate in the European Union gains speed. However, if the vaccination roll-out stalls more than we assume, the lifting of restrictions has to be delayed proportionally. In such a slowdown, the total number of cases and deaths until the end of the vaccination period increases accordingly. Thus, cautious lifting of restrictions and a fast vaccination delivery is essential to reduce death tolls and promptly increase freedom.

The spreading dynamics after concluding vaccination campaigns (Fig. 4 B,C) will be mainly determined by i) final vaccine uptake, ii) the contact network structure, iii) vaccine effectiveness, and iv) initial seroprevalence. Regarding vaccine uptake, we assumed that after the vaccination of every willing person, no further people would get vaccinated. This assumption enables us to study the effects of each parameter separately. However, vaccination willingness might change over time: it will probably be higher if reported case numbers and deaths are high, and vice versa. This poses a fundamental challenge: If low case numbers are maintained during the vaccine roll-out, the overall uptake might be comparably low, thus leading to a more severe wave once everyone has received a vaccination offer and restrictions are fully lifted. In contrast, a severe wave during vaccine roll-out might either increase vaccine uptake, because of individuals looking to protect themselves, or reduce it, because of damaged credibility on vaccine efficacy among vaccine hesitant groups. Thus, to avoid any further wave, policymakers have to maintain low case numbers *and* foster high vaccine uptake.

Besides vaccine uptake, the population's contact network also determines whether population immunity will be reached. We studied different real-world and theoretical possibilities for the contact matrices in Germany and other EU countries (cf. Fig. 7) and evaluated how our results depend on the connectivity among age groups. For the long-term success of the vaccination programs, there must be exceptionally sensible planning of measures to prevent contagion among school-aged children. Otherwise, they could become the drivers of a novel wave because they might remain mostly unvaccinated. Provided adequate vaccine uptake among the adult population, our results suggest that reducing either the intensity of contacts or the infectiousness in that age group by half would be sufficient for preventing a rebound wave. This reduction is attainable by implementing soft-distancing measures, plus systematic, preventive random screening with regular COVID-19 rapid tests in school settings or via vaccination [22]. Although at the time of writing some vaccines have been provisionally approved for use in children aged 12–15 years old, vaccine uptake among children remains highly uncertain because of their very low risk for severe illness from COVID-19. We therefore did not include their vaccination in our model.

One of the largest uncertainties regarding the dynamics after vaccine roll-out arises from the efficacies of the vaccines. First, the sterilizing immunity effect (i.e., blocking the transmission of the virus), is still not well quantified and understood [24]. Second, the emergence of new viral variants that at least partially escape immune response is continuously under investigation [35,37,38]. Furthermore, there is no certainty about whether escape variants might produce a more severe course of COVID-19 or whether reinfections with novel variants of SARS-CoV-2 would be milder. Therefore, we cannot conclusively quantify the level of contact reductions necessary in the long term to avoid a further wave of infections or whether such wave would overwhelm ICUs. However, for our default parameters, moderate contact reductions and hygiene measures would be sufficient to prevent further waves.

Although most examples are presented for countries from the European Union, our results can also be generalized to other countries. Differences across countries come from i) demographics, ii) varying seroprevalence—which originated from large differences in the severity of past waves—, iii) vaccines (types, availability, delivery scheme, and uptake), as well as iv) capacities of the health systems, including hospitals and TTI capabilities. For the EU, we find that during the mass vaccination phase, all these differences have only a minor effect on the pace at which restrictions can be lifted (cf. Supplementary Fig S1). However, differences become evident in the long term when most restrictions are lifted by the end of the vaccination campaigns. Demographics and contact patterns are qualitatively very similar across EU countries (cf. Fig. 7) and thus do not strongly change the expected outcome. On the contrary, we found the initial seroprevalence to significantly determine the minimum vaccine uptake required to guard against further waves after the vaccine roll-out (cf. Fig. 5). Naturally acquired immunity, like vaccinations, contributes to reducing the overall susceptibility of the population and thus impedes viral spread. Notably, naturally acquired immunity can compensate for drops in vaccine uptake in specific age groups unwilling to vaccinate or that cannot access the vaccine, e.g. in children. Furthermore, expected vaccine uptake considerably varies across EU countries (e.g., Serbia 38%, Croatia 41%, France 44%, Italy 70%, Finland 81% [6], Czech Republic 40% [39], Germany 80% [26]). The risk of rebound waves after the mass vaccinations might thus be highly heterogeneous across the EU.

Since we neither know what kind of escape variants might still surface nor their potential impact on vaccine efficacies or viral spread, maintaining low case numbers is the safest strategy for long-term planning. This strategy i) prevents avoidable deaths during vaccine roll-out, ii) offers better preparedness should escape variants emerge, and iii) lowers the risk of further waves because local outbreaks are easier to contain with efficient TTI. Hence, low case numbers only have advantages for health, society, and the economy. Furthermore, a low case number strategy would greatly profit from an EU-wide commitment, and coordination [15]. Otherwise, strict border controls with testing and quarantine policies need to be installed as drastically different case numbers between neighboring countries or regions promote destabilization; infections could (and will) propagate between countries triggering a “ping-pong” effect, especially if restrictions are not jointly planned. Therefore, promoting a high vaccine uptake and low case numbers strategy should not only be a priority for each country but also for the whole European community.

In practice, there are several ways to lower case numbers to the capacity limit of TTI programs without the need to enact stringent NPIs immediately. For example, if restrictions are lifted gradually but marginally slower than the rate vaccination pace would allow, case numbers will still decline. Alternatively, restrictions could be relaxed initially to an intermediate level where case numbers do not grow exponentially while giving people some freedom. In such circumstances one can take advantage of the reduced susceptibility to drive case numbers down without the need of stringent NPIs (Supplementary Fig S5 E–H).

To conclude, the opportunity granted by the progressing vaccination should not only be used to lift restrictions carefully but also to bring case numbers down. This will significantly reduce fatalities, allow to lift all major restrictions gradually moving into summer 2021, and guard against newly-emerging variants or potential further waves in the EU.

Methods

Model overview

We model the spreading dynamics of SARS-CoV-2 following a SEIRD-ICU deterministic formalism through a system of delay differential equations. Our model incorporates age-stratified dynamics, ICU stays, and the roll-out of a 2-dose vaccine. For a graphical representation of the infection and core dynamics, see Fig. 6. The contagion dynamics include the effect of externally acquired infections as a non-zero influx Φ_i based on the formalism previously developed by our group [18, 19]: susceptible individuals of a given age group i (S_i) can acquire the virus from infected individuals from any other age group j and subsequently progress to the exposed ($S_i \rightarrow E_i$) and infectious ($E_i \rightarrow I_i$) compartments. They can also acquire the virus externally. However, in this case, they progress directly to the infectious compartment ($S_i \rightarrow I_i$), i.e., they get infected abroad, and by the time they return, the latent period is already over. Individuals exposed to the virus (E_i) become infectious after the latent period and thus progress from the exposed to the infectious compartments (I_i) at a rate ρ ($E_i \rightarrow I_i$). The infectious compartment has three different possible transitions: i) direct recovery ($I_i \rightarrow R_i$), ii) progression to ICU ($I_i \rightarrow ICU_i$) or iii) direct death ($I_i \rightarrow D_i$). Individuals receiving ICU treatment can either recover ($ICU_i \rightarrow R_i$) or decrease ($ICU_i \rightarrow D_i$).

A contact matrix weights the infection probability between age groups. We investigated three different settings for the contact structure to assess its impact on the spreading dynamics of COVID-19: i) Interactions between age groups are proportional to the group size, i.e., the whole population is mixed perfectly homogeneously, ii) interactions are proportional to pre-COVID contact patterns in the EU population [28], and iii) interactions are proportional to “almost” pre-COVID contact patterns [28], i.e., the contact intensity in the youngest age group (0–19 years) is halved. This accounts for some preventive measures kept in place in schools, e.g., regular rapid testing or smaller class sizes. Scenario iii) is the default scenario unless explicitly stated. However, figures for scenarios i) and ii) are provided in the Supplementary Information. We scale all the contact structures by a linear factor, which increases or decreases the stringency of NPIs so that the settings are comparable. However, the scaling above does not account for heterogeneous NPIs acting only on contacts between specific age groups, such as workplace or school restrictions.

Our model includes the effect of vaccination, where vaccines are administered with an age-stratified two-dosage delivery scheme. The scheme does not discriminate on serological status, i.e., recovered individuals with natural antibodies may also access the vaccine when offered to them. Immunization, understood as the development of proper antibodies against SARS-CoV-2, does not occur immediately after receiving the vaccination dose. Thus, newly vaccinated individuals get temporarily put into extra compartments (V_i^0 and V_i^1 for the first and second dose respectively) where, if infected, they would progress through the disease stages as if they would not have received that dose. For modeling purposes, we assume that a sufficient immune response is build up τ days after being vaccinated ($V_i^0 \rightarrow S_i^1$ and $V_i^1 \rightarrow S_i^2$), and that a fraction $p_i(t)$ of those individuals that received the dose acquire the infection before being immunized. Furthermore, there is some evidence that the vaccines partially prevent the infection with and transmission of the disease [40, 41]. Our model incorporates the effectiveness against infection following an ‘all-or-nothing’ scheme, removing

a fraction of those vaccinated individuals to the recovered compartments ($V_i^0 \rightarrow R_i^1$ and $V_i^1 \rightarrow R_i^2$), thus assuming that they would not participate in the spreading dynamics. However, we consider those vaccinated individuals with a breakthrough infection have a lower probability of going to ICU or to die than unvaccinated individuals, i.e., effectiveness against severe disease follows a 'leaky' scheme. Furthermore, we assume those individuals carry a lower viral load and thus are less infectious by a factor of two [25]. All parameters and values are listed in Table 5.

We model the mean-field interactions between compartments by transition rates, determining the timescales involved. These transition rates can implicitly incorporate both the time course of the disease and the delays inherent to the case-reporting process. In the different scenarios analyzed, we include a non-zero influx Φ_i , i.e., new cases that acquired the virus from outside. Even though this influx makes a complete eradication of SARS-CoV-2 impossible, different outcomes in the spreading dynamics might arise depending on both contact intensity and TTI [18]. Additionally, we include the effects of non-compliance and unwillingness to be vaccinated as well as the effects of the TTI capacities from health authorities, building on [19]. Throughout the manuscript, we do not make explicit differences between symptomatic and asymptomatic infections. However, we implicitly consider asymptomatic infections by accounting for their effect on modifying the reproduction number R_t and all other epidemiological parameters. To assess the lifting of restrictions in light of progressing vaccinations, we use a Proportional-Derivative (PD) control approach to adapt the internal reproduction number R_t targeting controlled case numbers or ICU occupancy.

Model equations

The contributions of the spreading dynamics and the age-stratified vaccination strategies are summarized in the equations below. They govern the infection dynamics between the different age groups, each of which is represented by their susceptible-exposed-infectious-recovered-dead-ICU (SEIRD+ICU) compartments for all three vaccination statuses. We assume a regime that best resembles the situation in Germany at the beginning of March 2021, and we estimate the initial conditions for the different compartments of each age group accordingly. Furthermore, we assume that neither post-infection immunity [42] nor the immunization obtained through the different dosages of the vaccine vanish significantly in the considered time frames. The spreading parameters completely determine the resulting dynamics (characterized by the different age- and dose-dependent parameters, together with the hidden reproduction number R_t) and the vaccination logistics.

All of the following parameters and compartments are shortly described in Table 5 and Table 6. Some of these are additionally elaborated in more detail in the following sections. Subscripts i in the equations denote the different age groups, while superscripts denote the vaccination status: unvaccinated (0 or none), immunized by one dose (1), or by two doses (2).

$$\frac{dS_i}{dt} = - \underbrace{\bar{\gamma} R_t S_i \sum_{j,\nu} C_{ji} \frac{\sigma^\nu I_j^\nu}{M_j}}_{\text{internal contagion}} - \underbrace{f_i^1(t) \frac{S_i}{S_i + R_i}}_{\text{administering first dose}} - \underbrace{\frac{S_i}{M_i} \Phi_i}_{\text{external contagion}} \quad (1)$$

$$\frac{dV_i^0}{dt} = - \underbrace{\bar{\gamma} R_t V_i^0 \sum_{j,\nu} C_{ji} \frac{\sigma^\nu I_j^\nu}{M_j}}_{\text{internal contagion}} + \underbrace{f_i^1(t) \frac{S_i}{S_i + R_i}}_{\text{administering first dose}} - \underbrace{f_i^1(t - \tau) \frac{S_i}{S_i + R_i} \Big|_{t-\tau}}_{\text{first dose showing effect}} (1 - p_i(t)) - \underbrace{\frac{V_i^0}{M_i} \Phi_i}_{\text{external contagion}} \quad (2)$$

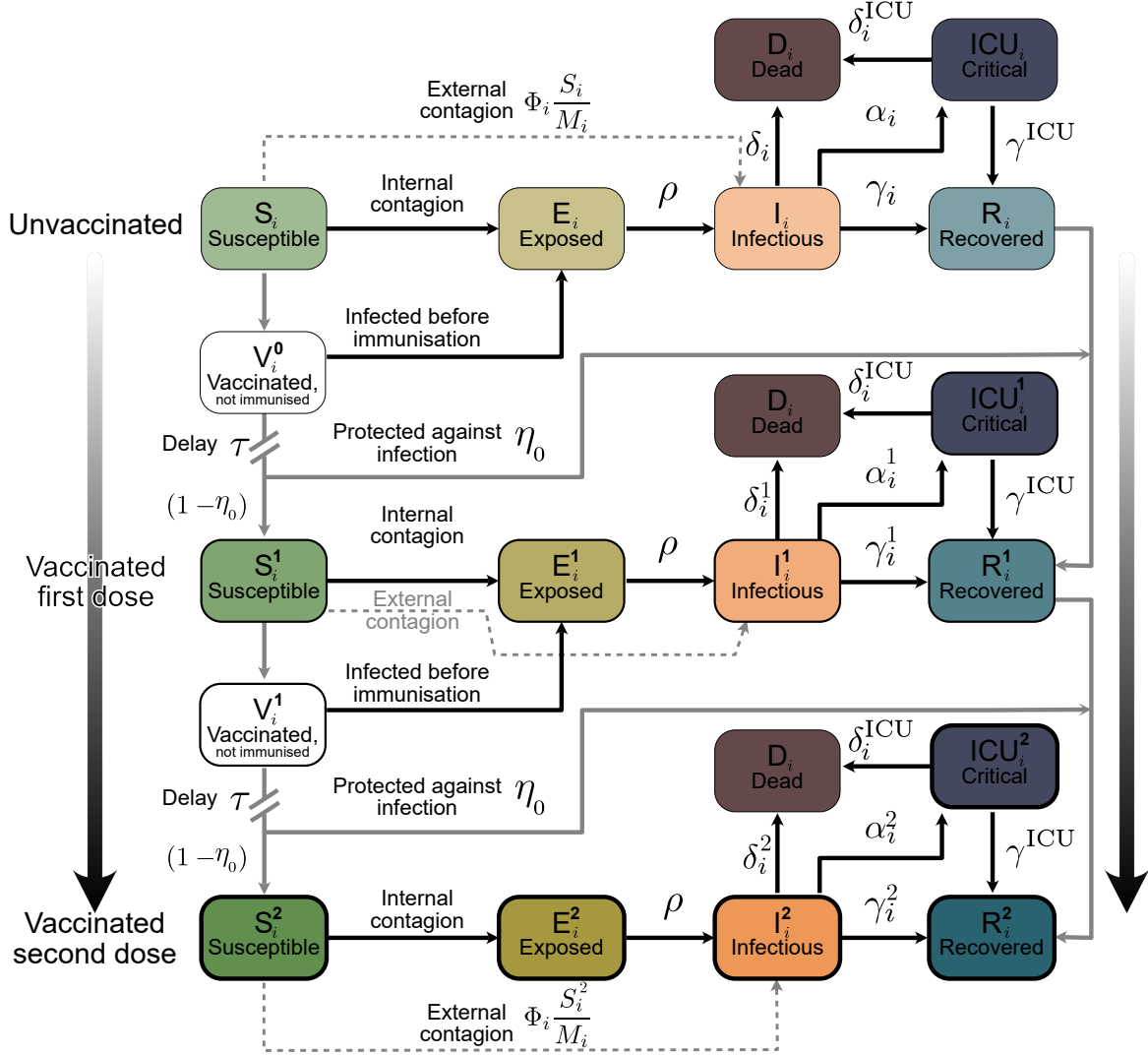


Figure 6: **Scheme of our age-stratified SEIRD-ICU+vaccination model.** The solid blocks in the diagram represent different SEIRD compartments. Solid black lines represent transition rates of the natural progression of the infection (contagion, latent period, and recovery). On the other hand, dashed lines account for external factors and vaccination. Solid gray lines represent non-linear transfers of individuals between compartments, e. g. through scheduled vaccination. From top to bottom, we describe the progression from unvaccinated to vaccinated, with stronger color and thicker edges indicating more protection from the virus. Subscripts i indicate the age groups, while superscripts represent the number of vaccine doses that have successfully strengthened immune response in individuals receiving them. Contagion can occur internally, where an individual from age group i can get infected from an infected person from any age group, or externally, e. g., abroad on vacation. If the contagion happens externally, we assume that the latent period is already over when the infected returns and, hence, they are immediately put into the infectious compartments I_i^ν .

$$\begin{aligned}
 \frac{dS_i^1}{dt} = & \underbrace{-\bar{\gamma}R_t S_i^1 \sum_{j,\nu} C_{ji} \frac{\sigma^\nu I_j^\nu}{M_j}}_{\text{internal contagion}} - \underbrace{f_i^2(t) \frac{S_i^1}{S_i^1 + R_i^1}}_{\text{administering second dose}} + \underbrace{(1 - \eta_0) f_i^1(t - \tau) \frac{S_i}{S_i + R_i} \Big|_{t-\tau}}_{\text{first dose (not immune)}} (1 - p_i(t)) - \underbrace{\frac{S_i^1}{M_i} \Phi_i}_{\text{external contagion}} \\
 & \hspace{15em} (3)
 \end{aligned}$$

$$\frac{dV_i^1}{dt} = \underbrace{-\bar{\gamma}R_t V_i^1 \sum_{j,\nu} C_{ji} \frac{\sigma^\nu I_j^\nu}{M_j}}_{\text{internal contagion}} + \underbrace{f_i^2(t) \frac{S_i^1}{S_i^1 + R_i^1}}_{\text{administering second dose}} - \underbrace{f_i^2(t-\tau) \frac{S_i^1}{S_i^1 + R_i^1} \Big|_{t-\tau}}_{\text{second dose showing effect}} (1 - p_i(t)) - \underbrace{\frac{V_i^1}{M_i} \Phi_i}_{\text{external contagion}} \quad (4)$$

$$\frac{dS_i^2}{dt} = \underbrace{-\bar{\gamma}R_t S_i^2 \sum_{j,\nu} C_{ji} \frac{\sigma^\nu I_j^\nu}{M_j}}_{\text{internal contagion}} + \underbrace{(1 - \eta_0) f_i^2(t-\tau) \frac{S_i^1}{S_i^1 + R_i^1} \Big|_{t-\tau}}_{\text{second dose (not immune)}} (1 - p_i(t)) - \underbrace{\frac{S_i^2}{M_i} \Phi_i}_{\text{external contagion}} \quad (5)$$

$$\frac{dE_i}{dt} = \underbrace{\bar{\gamma}R_t (S_i + V_i^0) \sum_{j,\nu} C_{ji} \frac{\sigma^\nu I_j^\nu}{M_j}}_{\text{internal contagion}} - \underbrace{\rho E_i}_{\text{end of latency}} \quad (6)$$

$$\frac{dE_i^1}{dt} = \underbrace{\bar{\gamma}R_t (S_i^1 + V_i^1) \sum_{j,\nu} C_{ji} \frac{\sigma^\nu I_j^\nu}{M_j}}_{\text{internal contagion}} - \underbrace{\rho E_i^1}_{\text{end of latency}} \quad (7)$$

$$\frac{dE_i^2}{dt} = \underbrace{\bar{\gamma}R_t S_i^2 \sum_{j,\nu} C_{ji} \frac{\sigma^\nu I_j^\nu}{M_j}}_{\text{internal contagion}} - \underbrace{\rho E_i^2}_{\text{end of latency}} \quad (8)$$

$$\frac{dI_i}{dt} = \underbrace{\rho E_i}_{\text{end of latency}} - \underbrace{\bar{\gamma}I_i}_{\text{recovery, ICU admission, or death}} + \underbrace{\frac{S_i + V_i^0}{M_i} \Phi_i}_{\text{external contagion}} \quad (9)$$

$$\frac{dI_i^1}{dt} = \underbrace{\rho E_i^1}_{\text{end of latency}} - \underbrace{\bar{\gamma}I_i^1}_{\text{recovery, ICU admission, or death}} + \underbrace{\frac{S_i^1 + V_i^1}{M_i} \Phi_i}_{\text{external contagion}} \quad (10)$$

$$\frac{dI_i^2}{dt} = \underbrace{\rho E_i^2}_{\text{end of latency}} - \underbrace{\bar{\gamma}I_i^2}_{\text{recovery, ICU admission, or death}} + \underbrace{\frac{S_i^2}{M_i} \Phi_i}_{\text{external contagion}} \quad (11)$$

$$\frac{dICU_i^\nu}{dt} = - \underbrace{(\delta_i^{\text{ICU}} + \gamma_i^{\text{ICU}}) ICU_i^\nu}_{\text{recovery or death}} + \underbrace{\alpha_i^\nu I_i^\nu}_{\text{ICU admission}} \quad (12)$$

$$\frac{dD_i}{dt} = \underbrace{\sum_\nu (\delta_i^{\text{ICU}} ICU_i^\nu + \delta_i^\nu I_i^\nu)}_{\text{total deaths}} \quad (13)$$

$$\frac{dR_i}{dt} = \underbrace{\gamma_i^{\text{ICU}} ICU_i + \gamma_i I_i}_{\text{recovery}} - \underbrace{f_i^1(t) \frac{R_i}{S_i + R_i}}_{\text{first dose}} \quad (14)$$

$$\frac{dR_i^1}{dt} = \underbrace{\gamma_i^{\text{ICU}} ICU_i^1 + \gamma_i^1 I_i^1}_{\text{recovery}} + \underbrace{f_i^1(t) \frac{R_i}{S_i + R_i}}_{\text{first dose after recovery}} - \underbrace{f_i^2(t) \frac{R_i^1}{S_i^1 + R_i^1}}_{\text{second dose}} + \underbrace{\eta_0 f_i^1(t-\tau) \frac{S_i}{S_i + R_i} \Big|_{t-\tau}}_{\text{first dose (sterilizing immunity)}} (1 - p_i(t)) \quad (15)$$

$$\frac{dR_i^2}{dt} = \underbrace{\gamma_i^{\text{ICU}} ICU_i^2 + \gamma_i^2 I_i^2}_{\text{recovery}} + \underbrace{f_i^2(t) \frac{R_i^1}{S_i^1 + R_i^1}}_{\text{second dose after recovery}} + \underbrace{\eta_0 f_i^2(t-\tau) \frac{S_i^1}{S_i^1 + R_i^1} \Big|_{t-\tau}}_{\text{second dose (sterilizing immunity)}} (1 - p_i(t)). \quad (16)$$

Contact structure and the effect of NPIs on the contact levels

We model the probability of a susceptible individual from age group i to get infected from an individual from age group j to be proportional to the –effective– incidence in that group ($\sum_{\nu} I_j^{\nu} \sigma^{\nu}$) and the contact intensity between the two groups, given by the entries $(C)_{ij}$ of a contact matrix C scaled with the gross reproduction number R_t . The contact matrices are normalized to force their largest eigenvalue (i.e., their spectral radius) to be 1, so that, when multiplied with R_t , their spectral radius equals R_t . The total contact levels for different levels of NPIs are then just linearly scaled with R_t . We thus neglect any inhomogeneities in the NPIs that might affect contact between specific age groups more than others.

As described previously, we study three different configurations for the contact matrix C : i) a perfectly homogeneously mixed population, ii) pre-COVID structure in the EU population [28], and iii) "almost" pre-COVID contact structure [28], but with reduced potentially-contagious contacts in the youngest age group (0–19 years) accounting for some preventive measures kept in place in schools. If not explicitly stated otherwise, the default contact matrix we use in the main text is always the intermediate "almost" pre-COVID contact structure matrix. For the three scenarios, we analyze the demographics and contact structures in Germany, Finland, the Czech Republic, and Italy as a sample for varying demographics across the EU.

First scenario: homogeneous contact structure. In this scenario, we consider that everyone has the same probability of meeting anyone from any other age group. The probability of meeting somebody from a given age group is thus proportional to the fraction of this age group within the whole population. Let f be the column vector collecting these fractions, $f_i = \frac{M_i}{M}$, the contact matrix for the n age-groups herein considered $C \in \mathbb{R}^{n \times n}$ is thus given by

$$(C)_{ij} = f_j, \forall j \tag{17}$$

and can be seen in Fig. 7 (A,D,G,J) for the chosen demographics. Note that by this construction the largest eigenvalue of this C (i.e., its spectral radius) is automatically 1 for any demographics, i.e. for any f that fulfills $\sum_j f_j = 1$ (proof in Supplementary Information).

Second scenario: pre-COVID contact intensity, real-world contact structure. Here, we use the whole contact matrices from before the pandemic reported with one-year age resolution in [28], converted into the age brackets that we chose. We normalize them by their spectral radius, leaving their internal contact structure intact. This scenario thus resembles completely homogeneous NPIs that affect every possible contact equally. The matrices are given in Fig. 7 (B,E,H,K) for the chosen countries.

Third scenario: "almost" pre-COVID contact intensity, real-world contact structure. Finally, we again use the contact matrices from before the pandemic reported in [28] but adapt them to reduce the intensity of contacts of the youngest age group by half, accounting for those measures that remain in place to prevent contagion and mitigate outbreaks in school settings. Specifically, we halve the matrix element connecting the 0–19 age group with itself and normalize the obtained contact matrix C by its spectral radius. As can be seen in the resulting matrices, given in Fig. 7 (C,F,I,L), this affects that the main contributions in the contacts are more evenly spread in the 0–59 year age groups. This serves as a first approximation to the contact structure with inhomogeneous NPIs targeting different age groups differently both in a complete lockdown, as well as some continued measures in schools.

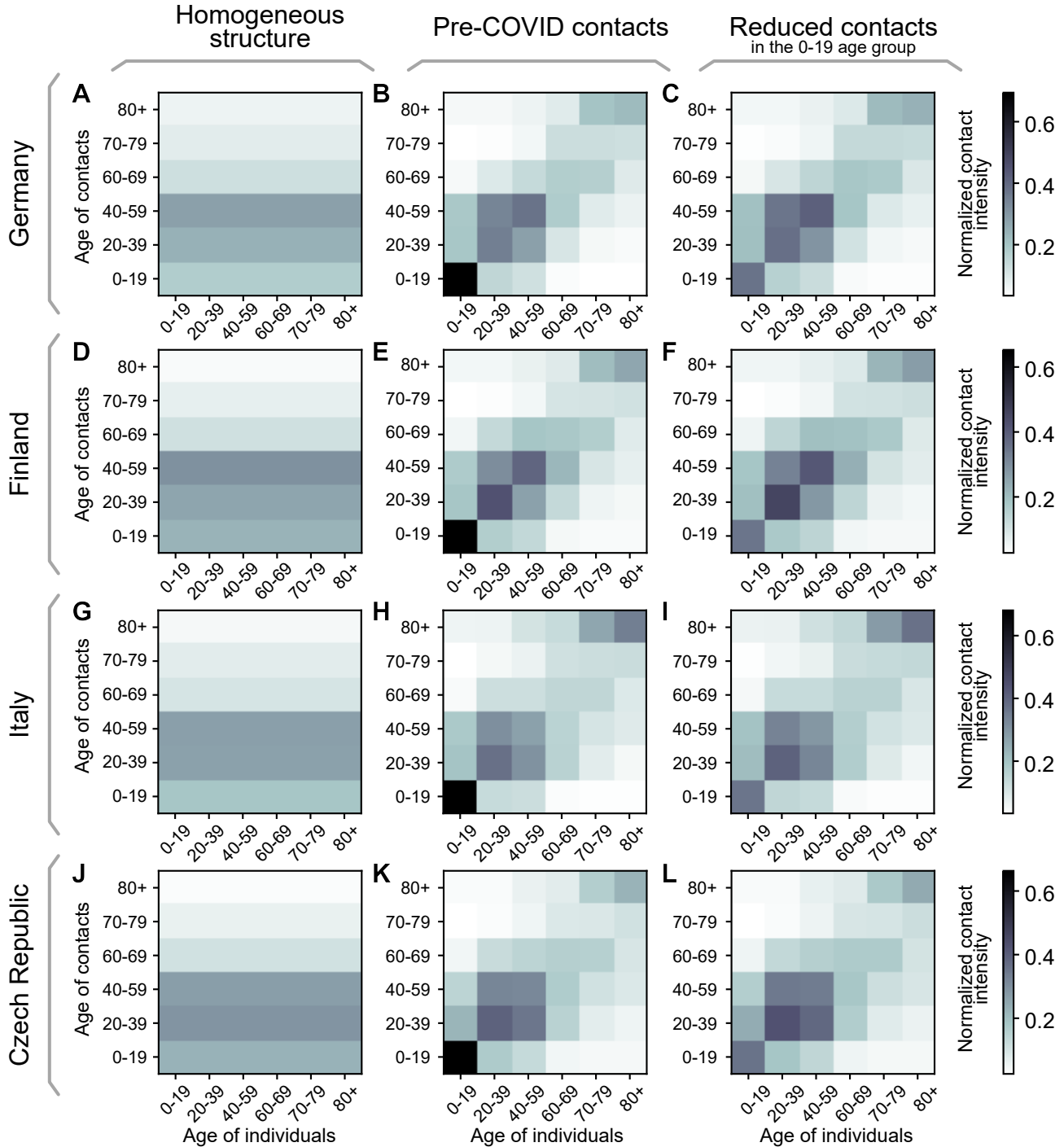


Figure 7: **Contact structures for different EU countries in the three scenarios.** The chosen contact matrices for i) homogeneous contact structure, ii) pre-COVID contact structure, and iii) "almost" pre-COVID structure with reduced potentially-contagious contacts in schools for Germany (A-C), Finland (D-F), Italy (G-I) and the Czech Republic (J-L). Entries of the matrices show the contact intensity between age groups normalized to give each matrix a spectral radius of 1.

Vaccination dynamics and logistics

In real-world settings, not every person accepts the vaccine when offered. Additionally, vaccine uptake is bounded because some vulnerable groups cannot be vaccinated because of health-related reasons. A

systematic survey [26] estimates the vaccine uptake to be approximately 80% across the adult population in Germany, which we chose as our baseline. Due to a higher perception of the risk caused by an infection, we expect that the uptake is higher for the elderly population. Thus, we set the uptake u_i to be age-group dependent. Besides the default 80%, we choose two more sets of uptakes averaging to a total of 70% and 90%, respectively. We suppose that an increase in the uptake is possible by education and information measures. They are listed in table 2. We linearly interpolate between the three to model arbitrary total vaccine uptakes.

Table 2: Parameters for the three main different vaccine uptake scenarios for Germany. The averages are to be understood across the vaccinable (16+) population. Slightly rescaled uptakes for Finnish, Italian and Czech age-demographics can be found in the Supplementary Information Tables S1–S3.

Group ID	age group	eligible fraction	minimal uptake u_i	mid uptake u_i (default)	maximal uptake u_i	population fraction [43] M_i/M
1	0-19	0.2 (16+)	0.58	0.73	0.88	0.18
2	20-39	1.0	0.64	0.76	0.89	0.25
3	40-59	1.0	0.69	0.79	0.90	0.28
4	60-69	1.0	0.74	0.82	0.91	0.13
5	70-79	1.0	0.79	0.86	0.92	0.09
6	>80	1.0	0.85	0.89	0.93	0.07
average			0.70	0.80	0.90	

Using official data of the German vaccine stock and stock projections [44, 45] we build up an estimated delivery function w_T that models the weekly number of doses delivered as a function of time. We assume it takes a logistic form, as we assume the number of daily doses increases strongly at the beginning until it reaches a stable level. Adapting the logistic function to the German stock projection (see Fig. 8) yields:

$$w_T(\text{week}) = \frac{11 \times 10^6 \text{ doses}}{1 + \exp(-0.17(\text{week} - 21))}, \quad (18)$$

where the parameters were chosen to roughly match past and projected deliveries, taking into account that some delays in the projections might appear because of logistic or manufacturing issues. Since the vaccine deliveries and distributions are done collectively and uniformly in the EU, we scale this German projection by the respective population sizes for the other countries studied herein (Finland, Italy, Czech Republic). We further assume that because of logistic delays, the vaccination of the delivered doses occurs with some delay, which we model as a convolution with an empirical delay kernel given by $K = [0.6, 0.3, 0.1]$ (fraction of vaccines administered in the same, second and third week following delivery). With that, we get the total vaccination rates per week.

These doses are distributed among the age groups, taking into account that each individual requires two doses, spaced by at least four weeks, aware of the potential benefits of further delaying the two doses [46].

The vaccine prioritization order is the following:

1. First, to meet the demand of second doses, τ_{vac} weeks after the first dose.
2. Second, to distribute a fraction v_r of the remaining doses uniformly among age groups, to model the earlier vaccination of exposed occupations (health sector, first responders, among others).

3. Last, to plan the rest of the doses for the oldest age group that has not been fully vaccinated yet.

Exceptions to rule 3 are the low-risk groups 16–19, 20–39, and 40–59 that get vaccinated simultaneously. For each age group, only a fraction u_i is vaccinated because of limited willingness to get vaccinated (Table 2). In addition, the total number of vaccinations in the youngest age group 0–19 is further reduced since we consider only a fraction of around 20% (fraction of 16–19 year-old individuals in the group) to be *eligible* for vaccination (see Table 2). The uptake u_i in this age group is thus understood only among the eligible individuals.

This procedure results in the number of first $w_i^1(\textit{week})$ and second doses $w_i^2(\textit{week})$ vaccinated to the age group i as function of the week. Dividing by 7 we obtain the daily administered first and second doses for age group i

$$f_i^1(t) = w_i^1(\lfloor t/7 \rfloor) / 7 \quad \text{and} \quad (19)$$

$$f_i^2(t) = w_i^2(\lfloor t/7 \rfloor) / 7. \quad (20)$$

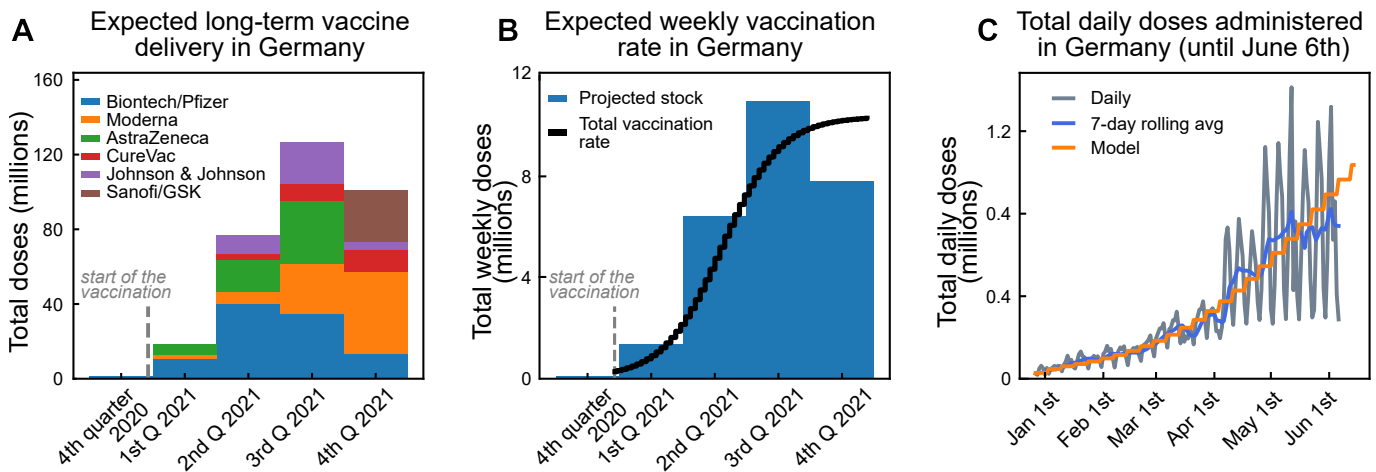


Figure 8: **Estimated vaccination rates for Germany.** From the announced vaccination stock, we estimate the vaccination delivery function. **A:** Total aggregated doses of different vaccine producers in Germany. **B:** Equivalent amount of 2-dose vaccines available per week in Germany, parameterized using a logistic function. **C:** Comparison between expected and observed vaccination progress in Germany.

Age-stratified transition rates

Here, we will introduce the transition rates used in the model equations; details about their estimation are presented in the later sections.

The recovery rate γ_i of a given age group describes the recovery without the need for critical care. It is estimated from the literature. We expect this parameter to vary across age groups, mainly because of the strong correlation between the severity of symptoms and age. Age-resolved recovery rates estimated from data of the non-vaccinated population in Germany are listed in Table 3.

The ICU recovery rate γ_i^{ICU} is the rate of a given age group for leaving ICU care. This parameter varies across age groups, mainly because of the strong correlation between the severity of symptoms, age, and duration of ICU stay. Age-resolved ICU recovery rates estimated from data of the non-vaccinated population in Germany are listed in Table 3.

Table 3: Age-dependent parameters

Group ID	ICU admission rate α_i (days ⁻¹)	Death rate in I δ_i (days ⁻¹)	Natural recovery rate γ_i (days ⁻¹)	Death rate in ICU δ_i^{ICU} (days ⁻¹)	ICU recovery rate γ_i^{ICU} (days ⁻¹)	Avg. duration in ICU $T_{\text{res}}^{\text{ICU}}$ (days)
1	0.000 014	0.000 002	0.099 98	0.005 560	0.194 440	5
2	0.000 204	0.000 014	0.099 78	0.007 780	0.192 220	5
3	0.001 217	0.000 111	0.098 67	0.006 164	0.084 745	11
4	0.004 031	0.000 317	0.095 65	0.009 508	0.081 401	11
5	0.005 435	0.001 422	0.093 14	0.019 756	0.091 355	9
6	0.007 163	0.004 749	0.088 09	0.082 433	0.084 233	6

The ICU admission rate α_i of a given age group describes the transition from the infected compartment to the ICU compartment. It accounts for those cases developing symptoms where intensive care is required and is estimated from the literature. We expect this parameter to vary across age groups, mainly because of the strong correlation between the severity of symptoms and age. Age-resolved ICU-transition rates estimated from data of the non-vaccinated population in Germany are listed in Table 3. Further, we assume that anyone requiring intensive care would have access to ICU beds and care.

The death rate δ_i also varies across age groups, mainly because of the strong correlation between the severity of symptoms and age. This parameter accounts for those individuals dying because of COVID-19, but without being treated in the ICU. In that way, it is expected to be even smaller than the infection fatality ratio (IFR). Age-resolved death rates (outside ICU) estimated from data of the non-vaccinated population in Germany are listed in Table 3.

The death rate in ICU δ_i^{ICU} also varies across age groups, mainly because of the strong correlation between the severity of symptoms and age. In addition, this parameter accounts for those individuals dying because of COVID-19 when being treated in the ICU. In that way, it is expected to be even larger than the case fatality ratio CFR. Age-resolved ICU death rates estimated from data of the non-vaccinated population in Germany are listed in Table 3.

We estimate these age-dependent rates by combining hospitalization data with published IFR data. A comparison of ICU transition rates α_i' across the EU is difficult as the definition of stationary treatment differs with regard to *hospitalization*, *ICU low* and *high-care*. In order to obtain sensible estimates for these rates, we need to consider the size of the unobserved pool in each age group. Our analysis of ICU transition rates is based on 14043 hospitalization reports collected in Germany between early 2020 and Oct. 26, 2020, as part of the official reporting data [47]. Those reports contain 20-year wide age strata but only represent a small sub-sample of all ICU-admissions ($n = 723$). A complete count of ICU-admissions is maintained by the *Deutsche Interdisziplinäre Vereinigung für Intensiv- und Notfallmedizin* [48], without additional patient-data, like age. 19250 ICU admissions were reported throughout the same time frame. We estimated the number of ICU admissions in each 20-year wide age group by combining both sources, matching well with German studies on the first wave [49].

Throughout the first and second wave, the per age-group case-fatality rates (CFRs) in Germany are more than two times larger than the age-specific infection fatality rates (IFRs) estimated by [27, 50]. This difference indicates unobserved infections. Seroprevalence studies from Q3 2020 [51] confirm the existence of unobserved

pools. The total number of infections in each age group is inferred from observed deaths assuming the age-specific IFR from [27]. α'_i (*low-* and *high-care*) is calculated by dividing estimated ICU-admissions in each age group by the estimated total infections in each of those groups. A similar method is applied for the ICU-death-rate δ_i^{ICU} by taking hospitalization-deaths from [47] as a proxy for the age distribution.

The ICU-rates from the 10-year wide age-groups [52] based on French data (*high-care* only) were used to subdivide the 20-year wide Age-group 60-79, replicating the French rate-ratio between 60-69 and 70-79 for the German ICU-ratios, while maintaining the German age-agnostic ICU-rate. Noteworthy, there is great variability between the reported ICU rates among different countries, and it seems to be more a problem of reporting criteria rather than differences in virus and host response [53]. Furthermore, as treatments become more effective compared to the first wave, the residence times have decreased in the second wave [30], thus modifying the transition rates.

We also considered the influence of our decision to use the IFR of O'Driscoll et al. [27] instead of Levin et al. [50]. The IFR from Levin et al. is about 50% larger and would lead to a lower level of infections overall in our scenarios, therefore reducing the fraction of natural immunity acquired at the end of the scenarios.

Estimation of general transition rates

After listing all transition rates that we consider in our work, we will now explain how we estimate them. Since we have to start somewhere, let us look at the ICU_i compartment first (see Fig. 6 top right). The differential equation, without influx and including the initial condition ICU_0 , is given by

$$\text{ICU}'_i = - \underbrace{\delta_i^{\text{ICU}} \text{ICU}_i}_{\text{to } D_i} - \underbrace{\gamma_i^{\text{ICU}} \text{ICU}_i}_{\text{to } R_i}, \quad \text{ICU}_i(0) = \text{ICU}_0. \quad (21)$$

The solution of this ODE is known to be

$$\text{ICU}_i = \text{ICU}_0 \exp(-(\delta_i^{\text{ICU}} + \gamma_i^{\text{ICU}})t). \quad (22)$$

If we know the average ICU_i residence time $T_{\text{res}}^{\text{ICU}}$, we can obtain an expression for $(\delta_i^{\text{ICU}} + \gamma_i^{\text{ICU}})$:

$$\delta_i^{\text{ICU}} + \gamma_i^{\text{ICU}} = \frac{1}{T_{\text{res}}^{\text{ICU}}}. \quad (23)$$

Further, assuming that a fraction f_δ of those individuals being admitted to ICUs would die, we obtain an expression linking all rates:

$$f_\delta = \frac{\# \text{ people dead by } t = \infty}{\text{people entering } \text{ICU}_i \text{ at } t = 0} = \frac{\delta_i^{\text{ICU}} \text{ICU}_0 \int_0^\infty \exp\left(-\frac{t}{T_{\text{res}}^{\text{ICU}}}\right) dt}{\text{ICU}_0} = \delta_i^{\text{ICU}} T_{\text{res}}^{\text{ICU}}. \quad (24)$$

Therefore, the transition rates are given by:

$$\delta_i^{\text{ICU}} = \frac{f_\delta}{T_{\text{res}}^{\text{ICU}}} \quad \text{and} \quad \gamma_i^{\text{ICU}} = \frac{(1 - f_\delta)}{T_{\text{res}}^{\text{ICU}}}. \quad (25)$$

Using this modeling approach, we implicitly assume the time scales at which people leave the ICU through recovery or death to be the same, i. e., the average ICU stay duration is independent of the outcome of the course of the disease.

Similarly, we can estimate the infected-to-death rate (δ_i), the infected-to-ICU transition rate (ICU admission rate α_i) and the infected-to-recovered rate (γ_i) based on these fractions and average times. If we assume that all the relevant median times are the same, we obtain the following expressions for the rates:

$$\delta_i = \frac{f_{I_i \rightarrow D_i}}{T_{\text{res}}^I}, \quad \alpha_i = \frac{f_{\text{ICU}}}{T_{\text{res}}^I}, \quad \gamma_i = \frac{(1 - (f_{I_i \rightarrow D_i} + f_{\text{ICU}}))}{T_{\text{res}}^I}. \quad (26)$$

As the average residence time in the I compartment is dominated by recoveries we assume $T_{\text{res}}^I = 10$ days [54–56].

Modeling vaccine efficacies

We assume the main effect of vaccinations on the individual to be twofold. A fraction η that has received both vaccine doses will develop total immunity and not contribute to the spreading dynamics. The rest may principally be infected with the virus but still have some protection against a severe course of the illness, resulting in a lower probability of dying or going to ICU. Both effects combined give the total protection against severe infections seen in vaccine studies, which we will denote with κ . For current COVID-19 vaccines, efficacies against severe disease κ ranging from 70–99% [23, 31–33, 57–59] and infection blocking potentials η of 60–90% [24, 41, 60, 61] are reported. The roughly uniform distribution of vaccine types in the European Union (see also Fig. 8), consists to a larger part of mRNA-type vaccines for which comparatively high values κ of 97–99% [33, 59] and η of 80–90% are reported. We thus chose the rather conservative 90% for κ and 75% for η as our default values. The explicit κ and η do not explicitly appear in our equations, but as parameters η_0 and κ_0 , which we derive from the reported numbers as follows.

Due to the lack of solid evidence on the effects of the first dose, we assume that the fraction of individuals developing total immunity already after the first dose is given by η_0 . We further assume that of the $(1 - \eta_0)$ people that do not develop the immunity after the first dose, the same fraction η_0 acquires it after the second dose, i. e. the total vaccination path of the people that do not develop total immunity after both doses is given by $S_i \xrightarrow{1-\eta_0} S_i^1 \xrightarrow{1-\eta_0} S_i^2$. η_0 can thus be related to η by the formula

$$\begin{aligned} \eta &= 1 - \frac{\text{not fully protected}}{\text{total vaccinated}} \\ &= 1 - (1 - \eta_0)^2 = \eta_0 (2 - \eta_0). \end{aligned} \quad (27)$$

For individuals vaccinated with both doses without total immunity, i. e., from S_i^2 , we reduce the probabilities to die or go to ICU after infection to account for the reduced risk of severe symptoms due to the vaccine. Of the total number of people who get vaccinated the risk of going to ICU or dying is thus reduced by a factor

$$(1 - \kappa) = (1 - \eta) \cdot (1 - \kappa_0), \quad (28)$$

from which we can deduce the value of κ_0 .

Again, due to lack of solid data on the first doses we assume the risk of severe COVID-19 is reduced to a factor $\sqrt{(1 - \kappa)}$ when only a single dose has been received. From these assumptions we arrive at

$$\delta_i^\nu = (\sqrt{1 - \kappa_0})^\nu \delta_i, \quad (29)$$

$$\alpha_i^\nu = (\sqrt{1 - \kappa_0})^\nu \alpha_i, \quad (30)$$

$$\gamma_i^\nu + \delta_i^\nu + \alpha_i^\nu = \bar{\gamma}, \quad (31)$$

where $\nu = \{1, 2\}$ represents the dose of the vaccine for which an individual has successfully developed antibodies. Note that ν is used as a super-index on the left-hand side of the equation but as an exponent on the right-hand side. Equation 31 enforces vaccination not to alter the total average timescale of the disease course.

The transition rates from ICU to death, δ_i^{ICU} , and from ICU to recovered, γ_i^{ICU} , are assumed to remain equal across doses. The reasons for this assumption are i) a lack of solid evidence for significant differences, and ii) once in ICU, it is reasonable to assume that the vaccine failed to work for this individual.

In addition to the effects of complete sterilizing immunity (η) and protection against severe disease (κ), we include a third effect of vaccines: Individuals that happen to have a breakthrough infection despite being vaccinated carry a lower viral load and are consequently less infectious than unvaccinated infected individuals. This has been shown already after the first dose [25, 60]. We include this effect by a factor σ in the contagion term (c.f. (1)).

Individuals becoming infectious while developing antibodies

One special case that one has to consider is when individuals acquire the virus in the time frame between being vaccinated and developing an adequate antibody level. We assume that individuals share behavioral characteristics with the members of the corresponding susceptible compartment, so contagion follows the same dynamics. Let $X_i(s)$ be the fraction of susceptible individuals of a given age group vaccinated at time $s_0 < s$ and are not infected until time s . Assuming they can only leave the compartment by getting infected, the differential equation governing their dynamics is:

$$\frac{dX_i}{ds} = -R_t X_i \sum_{j,\nu} C_{ji} \frac{\sigma^\nu I_j^\nu}{M_j} - \frac{X_i}{M_i} \Phi_i, \quad \text{with } X_i(s_0) = 1. \quad (32)$$

The solution of (32) is given by $X_i(s) = \exp\left(-\int_{s_0}^s \sum_{j,\nu} R_{s'} C_{ji} \frac{\sigma^\nu I_j^\nu(s')}{M_j} ds'\right) \exp\left(-\frac{\Phi_i(s-s_0)}{M_i}\right)$. Following the same formalism for every batch of vaccinated individuals produced at time $t - \tau$, the ones that remain susceptible by time t are given by:

$$X_i(t) = \exp\left(-\int_{t-\tau}^t \sum_{j,\nu} R_{t'} C_{ji} \frac{\sigma^\nu I_j^\nu(t')}{M_j} dt'\right) \exp\left(-\frac{\Phi_i \tau}{M_i}\right). \quad (33)$$

Therefore, we define the fraction of susceptible individuals acquiring the virus in the time-frame of antibodies development as

$$p_i(t) = 1 - \exp\left(-\int_{t-\tau}^t \sum_{j,\nu} R_{t'} C_{ji} \frac{\sigma^\nu I_j^\nu(t')}{M_j} dt'\right) \exp\left(-\frac{\Phi_i \tau}{M_i}\right). \quad (34)$$

This fraction is then subtracted in the transitions $V_i^\nu \rightarrow S_i^{\nu+1}$ from the vaccinated to the immunized pools in the differential equations.

Effect of test-trace-and-isolate

At low case numbers and moderate contact reduction, the spreading dynamics can be mitigated through test-trace-and-isolate (TTI) policies [18, 19]. In such a regime, individuals can have slightly more contacts because the overall low amount of cases enables a diligent system to trace offspring infections and stop the contagion chain. In other words, efficient TTI would allow for having a larger gross reproduction number R_t without rendering the system unstable. The precise allowed increase in R_t is determined by i) the rate at which symptomatic individuals are tested, ii) the probability of being randomly screened, and iii) the maximum capacity and fraction of contacts that health authorities can manually trace. When the different components of this meta-stable regime break down, we observe a self-accelerating growth in case numbers.

In our age-stratified model, we do not explicitly include TTI, given all the uncertainties that arise from the age-related modifying factors. However, we use our previous results to estimate the gross reproduction number R_t that would produce the same observed reproduction number in the different regimes of i) no test or contact tracing, ii) strict testing criteria, iii) self-reporting, and iv) full TTI. Doing so, we build an empirical relation to evaluating the contextual stringency of the different strategies herein compared (namely, long-term stabilization at high or low case numbers).

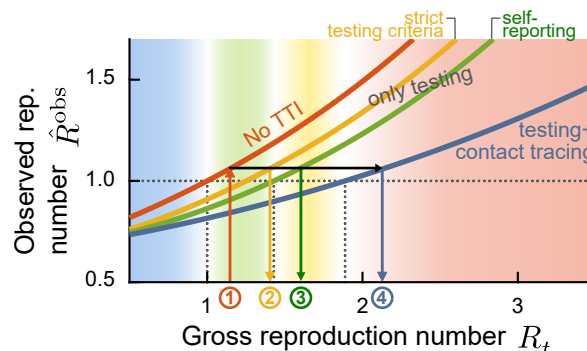


Figure 9: **Test-trace-and-isolate (TTI) policies allow for greater freedom (quantified by the gross reproduction number R_t) while observing the same reproduction number \hat{R}_t^{obs} .** Systematic efforts to slow down the spread of the disease, such as mass testing (random screening) and contact tracing, allow decreasing the observed reproduction number of the disease. For observing the same outcome in \hat{R}_t^{obs} , the gross reproduction number R_t would increase, or, in other words, individuals would be allowed to increase their potentially contagious contacts. Therefore, we extrapolate the R_t allowed in a full TTI setting at low case numbers and determine the equivalent R_t trends required to reach the same \hat{R}_t^{obs} in different regimes, starting from the raw value considering no TTI (red curve). Assuming that the relationship between R_t and \hat{R}_t^{obs} is exponential (eq (35)), we can obtain the expected R_t trends in the low-case numbers TTI regime. Starting from the raw R_t curve (red, 1), we can obtain R_t in all the other possible regimes: under strict testing criteria (yellow, 2), self-reporting (green, 3), or full TTI (blue, 4). Adapted from [18].

In the phase diagram of Fig. 9 we illustrate the conversion methodology. Two different R_t might produce the same observed reproduction number \hat{R}_t^{obs} , depending on the regime in which they operate. Fitting all curves

to an exponential function, and assuming that the largest eigenvalue of the system (for all possibilities of testing and tracing) can be represented as a function of the gross reproduction number R_t , we obtain

$$\hat{R}_t^{\text{obs}} = a \exp(bR_t). \quad (35)$$

We then want to evaluate how to translate the values we get from our control problem (which has no testing nor tracing) to the equivalent in other regimes. Assuming that all strategies have the same \hat{R}_t^{obs} (as schematized in Fig. 9), we can relate their gross reproduction numbers in each regime through a simple equation:

$$R_t^i = \frac{1}{b_i} \left(\ln \left(\frac{a_0}{a_i} \right) + b_0 R_t \right), \quad (36)$$

which corresponds to a line, and where the subscript 0 represents the base scenario (with no testing or contact tracing) and the subscript i represents the other strategies. The exponential fit to the curves shown in Fig. 9 gives to the following line equations:

$$R_t^{\text{test(ineff)}} = 1.0211R_t + 0.2229, \quad (37)$$

$$R_t^{\text{test(eff)}} = 1.0756R_t + 0.3272, \quad (38)$$

$$R_t^{\text{TTI}} = 1.6842R_t + 0.1805. \quad (39)$$

Assuming smooth transitions for these conversions in R_t , which are related to certain values the new daily cases N ($N_{\text{TTI}} < N_{\text{test(eff)}} < N_{\text{test(ineff)}} < N_{\text{no test}}$ respectively), we can define a general conversion $R_t(N)$:

$$R_t(N) = \begin{cases} R_t^{\text{TTI}}, & \text{if } N < N_{\text{TTI}} \\ R_t^{\text{test(eff)}} \phi_1 + R_t^{\text{TTI}} (1 - \phi_1), & \text{if } N_{\text{TTI}} \leq N < N_{\text{test(eff)}} \\ R_t^{\text{test(ineff)}} \phi_2 + R_t^{\text{test(eff)}} (1 - \phi_2), & \text{if } N_{\text{test(eff)}} \leq N < N_{\text{test(ineff)}} \\ R_t \phi_3 + R_t^{\text{test(ineff)}} (1 - \phi_3), & \text{if } N_{\text{test(ineff)}} \leq N < N_{\text{no test}} \\ R_t, & \text{else,} \end{cases} \quad (40)$$

where the ϕ parameters of each convex combination depend on N :

$$\phi_1 = \frac{N - N_{\text{TTI}}}{N_{\text{test(eff)}} - N_{\text{TTI}}}, \quad \phi_2 = \frac{N - N_{\text{test(eff)}}}{N_{\text{test(ineff)}} - N_{\text{test(eff)}}}, \quad \text{and} \quad \phi_3 = \frac{N - N_{\text{test(ineff)}}}{N_{\text{no test}} - N_{\text{test(ineff)}}}. \quad (41)$$

Default reference values for the N -related set-points are $N_{\text{TTI}} = 20$, $N_{\text{test(eff)}} = 100$, and $N_{\text{test(ineff)}} = 500$ and $N_{\text{no test}} = 10\,000$ new daily cases per million. When we plot and refer to the gross reproduction number R_t , it is always the value obtained from eq. (40).

Observed reproduction number

In real-world settings, the full extent of the disease spread can only be observed through testing and contact tracing. While the *true* number of daily infections N is a sum of all new infections in the hidden and traced pools, the *observed* number of daily infections \hat{N}^{obs} is the number of new infections discovered by

testing, tracing, and surveillance of the quarantined individuals' contacts. Thus, the observed number of daily infections is given by

$$\hat{N}^{\text{obs}}(t) = \left[\underbrace{\sum_{i,\nu} \rho E_i^\nu(t)}_{\text{end of latency}} + \underbrace{\sum_{i,\nu} \frac{S_i^\nu(t) + V_i^\nu(t)}{M_i} \Phi_i(t)}_{\text{ext. influx}} \right] \underbrace{\otimes \mathcal{K}(t)}_{\text{delay kernel}} \quad (42)$$

where \otimes denotes a convolution and \mathcal{K} an empirical probability mass function that models a variable reporting delay, inferred from German data. As the Robert-Koch-Institute (RKI), the official body responsible for epidemiological control in Germany [62], reports the date the test is performed, the delay until the appearance in the database can be inferred. The laboratories obtain 50 % of the sample results on the next day, 30 % the second day, 10 % the third day, and further delays complete the remaining 10 %, which for simplicity we will truncate at day four. Considering that an extra day is needed for reporting the laboratory results, the probability mass function for days 0 to 5 is given by $\mathcal{K} = [0, 0, 0.5, 0.3, 0.1, 0.1]$.

The spreading dynamics are usually characterized by the observed reproduction number \hat{R}_t^{obs} , an estimator of the effective reproduction number, calculated from the observed number of new cases $\hat{N}^{\text{obs}}(t)$. We use the definition underlying the estimates that are published by the RKI, which defines the reproduction number as the relative change of daily new cases separated by 4 days (the assumed serial interval of COVID-19 [63])

$$\hat{R}_t^{\text{obs}} = \frac{\hat{N}^{\text{obs}}(t)}{\hat{N}^{\text{obs}}(t-4)}. \quad (43)$$

In contrast to the original definition of \hat{R}_t^{obs} [62], we do not need to remove real-world noise effects by smoothing this ratio. It should be noted that calling \hat{N}^{obs} the observed case numbers is somewhat misleading since we do not model the hidden figure explicitly. However, as this is expected only to change slowly, it is still sufficiently accurate to obtain the observed reproduction number from eq. (43).

Keeping a steady number of daily infections with a PD control approach

With increasing immunity from the progressing vaccination program, keeping the spread of COVID-19 under control will require less and less effort by society. We can use this positive effect to lower the infections by upholding the same NPIs or gradually lifting restrictions to keep daily case numbers or ICU occupancy constant.

We model the optimal lifting of restrictions in the latter strategy using a Proportional Derivative (PD) control approach. The hidden reproduction number R_t is changed at every day of the simulation depending on either the daily case numbers \hat{N}^{obs} or the total ICU occupancy $\sum_{i,\nu} \text{ICU}_i^\nu$ such that the system is always driven towards a given set point. The change in R_t is negatively proportional to both the difference between the state and the setpoint as well as the change of that difference in time. The former dependence increases the number of infections if the case numbers drift down while the latter punishes rapid increases of the case numbers, keeping the system from overshooting the target value. We omit a dependence on the cumulative error, as is usually done in a PID controller, as that would enforce oscillations around the setpoint and because the PD has proven to be sufficient for our purposes.

Since both the case numbers and the ICU occupancy inherently only react to changes in R_t after a few days of delay, we can further improve the stability of the control by “looking into the future”. The full procedure for every day t of the simulation then follows:

1. Run the system for a time span T using the current R_t .
2. Quantify the relative error $\Delta(t + T)$ of the system state at the end by the difference between the observed case numbers or the total ICU occupancy and the chosen set point divided by said set point.
3. Calculate R_t for the next day according to

$$R_{t+1 \text{ day}} = R_t - \left(k_p \cdot \Delta(t + T) + k_d \cdot \frac{d\Delta}{dt}(t + T) \right),$$

where k_p and k_d denote constant control parameters listed in table 4.

4. Revert the system from the state at $t + T$ to $t + 1$ day and start again at 1.

We use the same control system to uphold the setpoint as we use to drive the system towards that state from the initial conditions. In a staged-control-like manner, we make the system more reactive to high slopes near the setpoint, i. e. increase k_d when within 10 % of the target. In this way, the system can drive up quickly to the target while preventing overreactions to the gradual immunization changes while hovering at the fixed value.

Scenarios 2-4 in the main text consist of a chain of these control problems, changing from controlled case numbers to controlled ICU occupancy at one of the vaccination milestones (Fig. 3).

Table 4: The PD control parameters depending on the objective

control problem	preview time span T	proportional k_p	derivative k_d
\hat{N}^{obs} (close to set point)	14 days	0.06	3.0
\hat{N}^{obs} (away from set point)	14 days	0.06	1.2
$\sum_{i,\nu} \text{ICU}'_i$ (close to set point)	14 days	0.2	15.0
$\sum_{i,\nu} \text{ICU}'_i$ (away from set point)	14 days	0.2	7.0

Parameter choices

For the age stratification of the population and the ICU rates, we used numbers published for Germany (Table 2). We suppose that the quantitative differences to other countries are not so large that the result would differ qualitatively. When comparing ICU rates across countries, one has to bear in mind that the definition of what constitutes an intensive care unit can differ between countries. We chose our ICU limit of 65 per million as a conservative limit so that in Germany, around three-quarters of the capacity would still be available for non-COVID patients. This limit was reached during the second wave in Germany. Other countries in the EU might have fewer remaining beds for non-COVID patients at this limit, as Germany has a comparatively high *per capita* number of ICU beds available.

ICU-related parameters are calculated from 14043 hospitalizations reported by German institutions until October 26, 2020 Table 3, converted to transitions rate from Table 1. All other epidemiological parameters, their sources, values, ranges, and units are listed in detail in Table 5.

The vaccine efficacy, as discussed previously, is modeled as a multiplicative factor of the non-vaccinated reference parameter. The dose-dependent multiplicative factor is chosen to be 90 % in the default scenario, which is in the range of the 70 to 95 % efficacy measured in phase 3 studies [57] of approved vaccines and in accordance to the 92% efficacy of the Pfizer vaccine found in a population study in Israel [23]. In addition, we analyzed different scenarios of vaccine uptake (namely, the overall compliance of people to get vaccinated according to the vaccination plan) because of its relevance to policymakers and different scenarios of the protection the vaccine grants against infections η . The latter has great relevance for assessing risks when evaluating restriction lifting.

Initial conditions

The initial conditions are chosen corresponding to the situation in Germany at the beginning of March 2021. We assume a seroprevalence of 10% because of post-infection immunity across all age groups, i.e., $R_i(0) = 0.1 \cdot M_i \forall i$. The vaccination at the beginning is according to the vaccination schedule introduced before, which leaves 5.1 million doses administered initially and an initial vaccination rate of 168 thousand doses per day. This compares to the 6.2 million total and the around 150 thousand daily administered doses at the time [26]. The initial number of daily new infections is at 200 per million, and the number of individuals treated in ICU is at 30 per million with an age distribution as observed during the first wave in Germany (taken from [47]). From these conditions and the total population sizes of the age groups (Table 2) we infer the initial size of each compartment.

Numerical calculation of solutions

The system of delay differential equations governing our model were numerically solved using a Runge-Kutta 4th order algorithm, implemented in Rust (version 1.48.0). The source code is available on GitHub https://github.com/Priesemann-Group/covid19_vaccination.

Author Contributions

S.B, S.C, J.D, and V.P. designed the research. S.B., S.C., and M.L. conducted the research. All authors analyzed the data. S.B. and S.C. created the figures. All authors wrote the paper.

Data availability

The source code for data generation and analysis is available online on GitHub https://github.com/Priesemann-Group/covid19_vaccination.

Acknowledgments

We thank the Priesemann group for exciting discussions and for their valuable input. We thank Christian Karagiannidis for fruitful discussions about the age-dependent hospitalization, ICU and fatality rates. All authors with affiliation (1) received support from the Max-Planck-Society. ÁO-N received funding from PIA-FB0001, ANID, Chile. ML, JD, SM received funding from the "Netzwerk Universitätsmedizin" (NUM) project egePan (01KX2021).

Table 5: Model parameters. The range column either describes the range of values used in the various scenarios, or if values depend on the age group (indexed by i), the lowest and highest value across age-groups.

Parameter	Meaning	Value (default)	Range	Units	Source
R_t	Reproduction number (gross)	1.00	0–3.5	–	Assumed
η	Vaccine protection against transmission	0.75	0.5–0.85	–	[24, 40, 41]
κ	Vaccine efficacy (against severe disease)	0.9	0.7–0.95	–	[23, 57]
σ^ν	Relative virulence of unvaccinated and vaccinated individuals	[1.0, 0.5, 0.5]	0.5 – 1	–	[25]
τ	Immunization delay	7		days	[24, 31]
v_r	Random vaccination fraction	0.35			[64, 65]
M_i	Population group size	Table 2		people	[43]
u_i	Vaccine uptake	Table 2		–	[6]
ρ	Transition rate $E \rightarrow I$	0.25		day ⁻¹	[66, 67]
γ_i^ν	Recovery rate from I_i^ν	Table 3	0.088 – 0.1	day ⁻¹	[54–56]
γ_i^{ICU}	Recovery rate from ICU $_i^\nu$	Table 3	0.08 – 0.2	day ⁻¹	[50, 52, 68]
δ_i^ν	Death rate from I_i^ν	Table 3	10 ⁻⁶ – 0.005	day ⁻¹	[50, 52, 68]
δ_i^{ICU}	Death rate from ICU $_i^\nu$	Table 3	0.0055 – 0.083	day ⁻¹	[50, 52, 68]
α_i^ν	Transition rate $I \rightarrow \text{ICU}$	Table 3	10 ⁻⁵ – 0.007	day ⁻¹	[50, 52, 68]
Φ_i	Infections from external sources	1		cases day ⁻¹ per million	Assumed
$p_i(t)$	Fraction of individuals getting infected before acquiring antibodies	–	–	–	Eq. (34)
$\bar{\gamma}$	Effective removal rate from infectious compartment	–	–	day ⁻¹	$(\gamma_i^\nu + \alpha_i^\nu + \delta_i^\nu)$
$f_i^1(t), f_i^2(t)$	Administered 1 st and 2 nd vaccine doses	–	–	doses/day	Eq. (19), (20)

Table 6: Model variables, Subscripts i denote the i th age group, superscripts the vaccination status (Unvaccinated, immunized by one dose, by two doses).

Variable	Meaning	Units	Explanation
S_i, S_i^1, S_i^2	Susceptible pools	people	Non-infected people that may acquire the virus.
V_i^0, V_i^1	Vaccinated pools	people	Non-infected people that have been vaccinated but have not developed antibodies yet, thus may acquire the virus.
E_i, E_i^1, E_i^2	Exposed pools	people	Infected people in latent period. Can not spread the virus.
I_i, I_i^1, I_i^2	Infected pools	people	Currently infectious people.
ICU_i, ICU_i^1, ICU_i^2	ICU pools	people	Infected people receiving ICU treatment, isolated.
D_i, D_i^1, D_i^2	Dead pools	people	Dead people.
R_i, R_i^1, R_i^2	Recovered pools	people	Recovered/immune people that have acquired post-infection or sterilizing vaccination immunity.
\hat{N}^{obs}	Observed new infections	people day ⁻¹	Daily new infections, including reporting delays. eq. (42)
\hat{R}_t^{obs}	Observed reproduction number	–	The reproduction number that can be estimated only from the observed cases: $\hat{R}_t^{\text{obs}} = \hat{N}^{\text{obs}}(t)/\hat{N}^{\text{obs}}(t-4)$.

References

- [1] Sebastian Contreras and Viola Priesemann. Risking further COVID-19 waves despite vaccination. *The Lancet Infectious Diseases*, 2021.
- [2] Brody H Foy, Brian Wahl, Kayur Mehta, Anita Shet, Gautam I Menon, and Carl Britto. Comparing COVID-19 vaccine allocation strategies in India: A mathematical modelling study. *International Journal of Infectious Diseases*, 103:431–438, 2021.
- [3] Sam Moore, Edward M Hill, Michael J Tildesley, Louise Dyson, and Matt J Keeling. Vaccination and non-pharmaceutical interventions for COVID-19: a mathematical modelling study. *The Lancet Infectious Diseases*, 2021.
- [4] Joao Viana, Christiaan H van Dorp, Ana Nunes, Manuel C Gomes, Michiel van Boven, Mirjam E Kretzschmar, Marc Veldhoen, and Ganna Rozhnova. Controlling the pandemic during the SARS-CoV-2 vaccination rollout: a modeling study. *Nature communications*, 12(3674):1–15, 2021.
- [5] Kate M Bubar, Kyle Reinholt, Stephen M Kissler, Marc Lipsitch, Sarah Cobey, Yonatan H Grad, and Daniel B Larremore. Model-informed COVID-19 vaccine prioritization strategies by age and serostatus. *Science*, 2021.
- [6] Olivier J Wouters, Kenneth C Shadlen, Maximilian Salcher-Konrad, Andrew J Pollard, Heidi J Larson, Yot Teerawattananon, and Mark Jit. Challenges in ensuring global access to COVID-19 vaccines: production, affordability, allocation, and deployment. *The Lancet*, 2021.

- [7] Nicholas G. Davies, Sam Abbott, Rosanna C. Barnard, Christopher I. Jarvis, Adam J. Kucharski, James D. Munday, Carl A. B. Pearson, Timothy W. Russell, Damien C. Tully, Alex D. Washburne, Tom Wenseleers, Amy Gimma, William Waites, Kerry L. M. Wong, Kevin van Zandvoort, Justin D. Silverman, CMMID COVID-19 Working Group¹‡, COVID-19 Genomics UK (COG-UK) Consortium[‡], Karla Diaz-Ordaz, Ruth Keogh, Rosalind M. Eggo, Sebastian Funk, Mark Jit, Katherine E. Atkins, and W. John Edmunds. Estimated transmissibility and impact of SARS-CoV-2 lineage B.1.1.7 in England. *Science*, March 2021.
- [8] Jessica A. Plante, Brooke M. Mitchell, Kenneth S. Plante, Kari Debbink, Scott C. Weaver, and Vineet D. Menachery. The variant gambit: COVID’s next move. *Cell Host & Microbe*, 2021.
- [9] Debra Van Egeren, Alexander Novokhodko, Madison Stoddard, Uyen Tran, Bruce Zetter, Michael Rogers, Bradley L Pentelute, Jonathan M Carlson, Mark Hixon, Diane Joseph-McCarthy, et al. Risk of rapid evolutionary escape from biomedical interventions targeting sars-cov-2 spike protein. *PloS one*, 16(4):e0250780, 2021.
- [10] Jennie S Lavine, Ottar N Bjornstad, and Rustom Antia. Immunological characteristics govern the transition of COVID-19 to endemicity. *Science*, 371(6530):741–745, 2021.
- [11] Anna Petherick, Rafael G Goldszmidt, Eduardo B Andrade, Rodrigo Furst, Anna Pott, and Andrew Wood. A worldwide assessment of COVID-19 Pandemic-Policy Fatigue. *Available at SSRN 3774252*, 2021.
- [12] Jay J Van Bavel, Katherine Baicker, Paulo S Boggio, Valerio Capraro, Aleksandra Cichocka, Mina Cikara, Molly J Crockett, Alia J Crum, Karen M Douglas, James N Druckman, et al. Using social and behavioural science to support COVID-19 pandemic response. *Nature Human Behaviour*, pages 1–12, 2020.
- [13] Jonas Dehning, Johannes Zierenberg, F Paul Spitzner, Michael Wibral, Joao Pinheiro Neto, Michael Wilczek, and Viola Priesemann. Inferring change points in the spread of COVID-19 reveals the effectiveness of interventions. *Science*, 2020.
- [14] Jan M. Brauner, Sören Mindermann, Mrinank Sharma, David Johnston, John Salvatier, Tomáš Gavenčiak, Anna B. Stephenson, Gavin Leech, George Altman, Vladimir Mikulik, Alexander John Norman, Joshua Teperowski Monrad, Tamay Besiroglu, Hong Ge, Meghan A. Hartwick, Yee Whye Teh, Leonid Chindelevitch, Yarin Gal, and Jan Kulveit. Inferring the effectiveness of government interventions against COVID-19. *Science*, 2020.
- [15] Viola Priesemann, Melanie M. Brinkmann, Sandra Ciesek, Sarah Cuschieri, Thomas Czypionka, Giulia Giordano, Deepti Gurdasani, Claudia Hanson, Niel Hens, Emil Iftekhar, Michelle Kelly-Irving, Peter Klimek, Mirjam Kretzschmar, Andreas Peichl, Matjaž Perc, Francesco Sannino, Eva Schernhammer, Alexander Schmidt, Anthony Staines, and Ewa Szczurek. Calling for pan-European commitment for rapid and sustained reduction in SARS-CoV-2 infections. *The Lancet*, 2020.
- [16] Florian Dorn, Sahamoddin Khailaie, Marc Stoeckli, Sebastian C. Binder, Berit Lange, Stefan Lautenbacher, Andreas Peichl, Patrizio Vanella, Timo Wollmershäuser, Clemens Fuest, and Michael Meyer-Hermann. The Common Interests of Health Protection and the Economy: Evidence from Scenario Calculations of COVID-19 Containment Policies. *medRxiv*, page 2020.08.14.20175224, August 2020.
- [17] Miquel Oliu-Barton, Bary SR Pradelski, Philippe Aghion, Patrick Artus, Ilona Kickbusch, Jeffrey V Lazarus, Devi Sridhar, and Samantha Vanderslott. SARS-CoV-2 elimination, not mitigation, creates best outcomes for health, the economy, and civil liberties. *The Lancet*, 2021.

- [18] Sebastian Contreras, Jonas Dehning, Matthias Loidolt, Johannes Zierenberg, F Paul Spitzner, Jorge H Urrea-Quintero, Sebastian B Mohr, Michael Wilczek, Michael Wibral, and Viola Priesemann. The challenges of containing SARS-CoV-2 via test-trace-and-isolate. *Nature communications*, 12(1):1–13, 2021.
- [19] Sebastian Contreras, Jonas Dehning, Sebastian B Mohr, F Paul Spitzner, and Viola Priesemann. Low case numbers enable long-term stable pandemic control without lockdowns. *medRxiv*, 2020.
- [20] Mirjam E. Kretzschmar, Ganna Rozhnova, and Michiel van Boven. Isolation and Contact Tracing Can Tip the Scale to Containment of COVID-19 in Populations With Social Distancing. *Frontiers in Physics*, 8, 2021.
- [21] Prakhar Godara, Stephan Herminghaus, and Knut M. Heidemann. A control theory approach to optimal pandemic mitigation. *PLOS ONE*, 16(2):1–16, 2021.
- [22] Mrinank Sharma, Sören Mindermann, Charlie Rogers-Smith, Gavin Leech, Benedict Snodin, Janvi Ahuja, Jonas B. Sandbrink, Joshua Teperowski Monrad, George Altman, Gurpreet Dhaliwal, Lukas Finnveden, Alexander John Norman, Sebastian B. Oehm, Julia Fabienne Sandkühler, Thomas Mellan, Jan Kulveit, Leonid Chindelevitch, Seth Flaxman, Yarin Gal, Swapnil Mishra, Jan Markus Brauner, and Samir Bhatt. Understanding the effectiveness of government interventions in Europe’s second wave of COVID-19. *medRxiv*, page 2021.03.25.21254330, March 2021.
- [23] Noa Dagan, Noam Barda, Eldad Kepten, Oren Miron, Shay Perchik, Mark A. Katz, Miguel A. Hernán, Marc Lipsitch, Ben Reis, and Ran D. Balicer. BNT162b2 mRNA COVID-19 Vaccine in a Nationwide Mass Vaccination Setting. *New England Journal of Medicine*, 2021.
- [24] Matan Levine-Tiefenbrun, Idan Yelin, Rachel Katz, Esma Herzel, Ziv Golan, Licita Schreiber, Tamar Wolf, Varda Nadler, Amir Ben-Tov, Jacob Kuint, et al. Initial report of decreased sars-cov-2 viral load after inoculation with the bnt162b2 vaccine. *Nature medicine*, 27(5):790–792, 2021.
- [25] Ross J. Harris, Jennifer A. Hall, Asad Zaidi, Nick J. Andrews, J. Kevin Dunbar, and Gavin Dabrera. Effect of vaccination on household transmission of sars-cov-2 in england. *New England Journal of Medicine*, 0(0):null, 0.
- [26] Robert Koch Institute. COVID-19 Impfquoten-Monitoring in Deutschland (COVIMO) –1. Report. https://www.rki.de/DE/Content/InfAZ/N/Neuartiges_Coronavirus/Projekte_RKI/covimo_studie_bericht_1.pdf, 2021.
- [27] Megan O’Driscoll, Gabriel Ribeiro Dos Santos, Lin Wang, Derek A. T. Cummings, Andrew S. Azman, Juliette Paireau, Arnaud Fontanet, Simon Cauchemez, and Henrik Salje. Age-specific mortality and immunity patterns of SARS-CoV-2. *Nature*, 590(7844):140–145, 2021.
- [28] Dina Mistry, Maria Litvinova, Ana Pastore y Piontti, Matteo Chinazzi, Laura Fumanelli, Marcelo FC Gomes, Syed A Haque, Quan-Hui Liu, Kunpeng Mu, Xinyue Xiong, et al. Inferring high-resolution human mixing patterns for disease modeling. *Nature communications*, 12(1):1–12, 2021.
- [29] RKI. Corona-Monitoring bundesweit (RKI-SOEP-Studie): Überblick zu ersten Ergebnissen. <https://www.rki.de/DE/Content/Gesundheitsmonitoring/Studien/lid/Ergebnisse.html?nn=14830934>, 2021.
- [30] Christian Karagiannidis, Wolfram Windisch, Daniel F McAuley, Tobias Welte, and Reinhard Busse. Major differences in ICU admissions during the first and second COVID-19 wave in germany. *The Lancet Respiratory Medicine*, 2021.

- [31] Fernando P. Polack, Stephen J. Thomas, Nicholas Kitchin, Judith Absalon, Alejandra Gurtman, Stephen Lockhart, John L. Perez, Gonzalo Pérez Marc, Edson D. Moreira, Cristiano Zerbini, Ruth Bailey, Kena A. Swanson, Satrajit Roychoudhury, Kenneth Koury, Ping Li, Warren V. Kalina, David Cooper, Robert W. Frenck, Laura L. Hammitt, Özlem Türeci, Haylene Nell, Axel Schaefer, Serhat Ünal, Dina B. Tresnan, Susan Mather, Philip R. Dormitzer, Uğur Şahin, Kathrin U. Jansen, and William C. Gruber. Safety and Efficacy of the BNT162b2 mRNA COVID-19 Vaccine. *New England Journal of Medicine*, 383(27):2603–2615, 2020. PMID: 33301246.
- [32] Merryn Voysey, Sue Ann Costa Clemens, Shabir A Madhi, Lily Y Weckx, Pedro M Folegatti, Parvinder K Aley, Brian Angus, Vicky L Baillie, Shaun L Barnabas, Qasim E Bhorat, et al. Safety and efficacy of the ChAdOx1 nCoV-19 vaccine (AZD1222) against SARS-CoV-2: an interim analysis of four randomised controlled trials in Brazil, South Africa, and the UK. *The Lancet*, 397(10269):99–111, 2021.
- [33] Israel Ministry of Health. Effectiveness Data of the COVID-19 Vaccine Collected in Israel until 13.2.2021. <https://www.gov.il/en/departments/news/20022021-01>. Last updated: 2021-02-22, Accessed: 2021-03-03.
- [34] Ella Petter, Orna Mor, Neta Zuckerman, Danit Oz-Levi, Asaf Younger, Dvir Aran, and Yaniv Erlich. Initial real world evidence for lower viral load of individuals who have been vaccinated by bnt162b2. *medRxiv*, 2021.
- [35] Daniel M. Altmann, Rosemary J. Boyton, and Rupert Beale. Immunity to SARS-CoV-2 variants of concern. *Science*, 371(6534):1103–1104, March 2021.
- [36] Pengfei Wang, Manoj S Nair, Lihong Liu, Sho Iketani, Yang Luo, Yicheng Guo, Maple Wang, Jian Yu, Baoshan Zhang, Peter D Kwong, et al. Antibody resistance of sars-cov-2 variants b. 1.351 and b. 1.1. 7. *Nature*, pages 1–6, 2021.
- [37] Wilfredo F. Garcia-Beltran, Evan C. Lam, Kerri St. Denis, Adam D. Nitido, Zeidy H. Garcia, Blake M. Hauser, Jared Feldman, Maia N. Pavlovic, David J. Gregory, Mark C. Poznansky, Alex Sigal, Aaron G. Schmidt, A. John Iafrate, Vivek Naranbhai, and Alejandro B. Balazs. Multiple SARS-CoV-2 variants escape neutralization by vaccine-induced humoral immunity. *Cell*, March 2021.
- [38] Alison Tarke, John Sidney, Nils Methot, Esther Dawen Yu, Yun Zhang, Jennifer M Dan, Benjamin Goodwin, Paul Rubiro, Aaron Sutherland, Eric Wang, et al. Impact of sars-cov-2 variants on the total cd4+ and cd8+ t cell reactivity in infected or vaccinated individuals. *Cell Reports Medicine*, page 100355, 2021.
- [39] David Hutt. Why are czechs among europe’s most sceptical over taking vaccines?, Jan 2021.
- [40] Smriti Mallapaty. Can COVID vaccines stop transmission? Scientists race to find answers. *Nature*, 2021.
- [41] Victoria Jane Hall, Sarah Foulkes, Ayoub Saei, Nick Andrews, Blanche Oguti, Andre Charlett, Edgar Wellington, Julia Stowe, Natalie Gillson, Ana Atti, Jasmin Islam, Ioannis Karagiannis, Katie Munro, Jameel Khawam, The SIREN Study Group, Meera A. Chand, Colin Brown, Mary E. Ramsay, Jamie Lopez Bernal, and Susan Hopkins. Effectiveness of BNT162b2 mRNA Vaccine Against Infection and COVID-19 Vaccine Coverage in Healthcare Workers in England, Multicentre Prospective Cohort Study (the SIREN Study). SSRN Scholarly Paper ID 3790399, Social Science Research Network, Rochester, NY, 2021.
- [42] Jennifer M. Dan, Jose Mateus, Yu Kato, Kathryn M. Hastie, Esther Dawen Yu, Caterina E. Faliti, Alba Grifoni, Sydney I. Ramirez, Sonya Haupt, April Frazier, Catherine Nakao, Vamseedhar Rayaprolu, Stephen A. Rawlings, Bjoern Peters, Florian Krammer, Viviana Simon, Erica Ollmann Saphire, Davey M.

- Smith, Daniela Weiskopf, Alessandro Sette, and Shane Crotty. Immunological memory to SARS-CoV-2 assessed for up to 8 months after infection. *Science*, 371(6529), 2021.
- [43] DESTATIS. 14. koordinierte Bevölkerungsvorausberechnung für Deutschland (Coordinated Population Projection for Germany). <https://service.destatis.de/bevoelkerungspyramide/#!a=70,80&l=en&g>, 2019. Bevölkerungspyramide: Altersstruktur Deutschlands von 1950 - 2060.
- [44] RKI. Digitales Impfquotenmonitoring zur COVID-19-Impfung. https://www.rki.de/DE/Content/InfAZ/N/Neuartiges_Coronavirus/Daten/Impfquoten-Tab.html, 2021.
- [45] Der Spiegel. Impfstoff für 50 Millionen bis Ende Juni, Feb 2021.
- [46] Benjamin F. Maier, Angelique Burdinski, Annika H. Rose, Frank Schlosser, David Hinrichs, Cornelia Betsch, Lars Korn, Philipp Sprengholz, Michael Meyer-Hermann, Tanmay Mitra, Karl Lauterbach, and Dirk Brockmann. Potential benefits of delaying the second mRNA COVID-19 vaccine dose, 2021.
- [47] J Schilling, AS Lehfeld, D Schumacher, A Ullrich, M Diercke, et al. Krankheitsschwere der ersten COVID-19-Welle in Deutschland basierend auf den Meldungen gemäß Infektionsschutzgesetz. *Journal of Health Monitoring*, 5(S11):2—20, 2020.
- [48] Intensivregister-Team am RKI. Tagesreport aus dem DIVI-Intensivregister. <https://doi.org/10.25646/7625>, 2020.
- [49] Christian Karagiannidis, Carina Mostert, Corinna Hentschker, Thomas Voshaar, Jürgen Malzahn, Gerhard Schillinger, Jürgen Klauber, Uwe Janssens, Gernot Marx, Steffen Weber-Carstens, et al. Case characteristics, resource use, and outcomes of 10 021 patients with COVID-19 admitted to 920 German hospitals: an observational study. *The Lancet Respiratory Medicine*, 8(9):853–862, 2020.
- [50] Andrew T Levin, William P. Hanage, Nana Owusu-Boaitey, Kensington B. Cochran, Seamus P. Walsh, and Gideon Meyerowitz-Katz. Assessing the age specificity of infection fatality rates for COVID-19: systematic review, meta-analysis, and public policy implications. *European Journal of Epidemiology*, 2020.
- [51] Claudia Santos-Hövenner, Markus A Busch, Carmen Koschollek, Martin Schlaud, Jens Hoebel, Robert Hoffmann, Hendrik Wilking, Sebastian Haller, Jennifer Allenj, Jörg Wernitz, et al. Seroepidemiological study on the spread of SARS-CoV-2 in populations in especially affected areas in Germany—Study protocol of the CORONA-MONITORING lokal study. *Journal of Health*, 2020.
- [52] Henrik Salje, Cécile Tran Kiem, Noémie Lefrancq, Noémie Courtejoie, Paolo Bosetti, Juliette Paireau, Alessio Andronico, Nathanaël Hozé, Jehanne Richet, Claire-Lise Dubost, et al. Estimating the burden of SARS-CoV-2 in France. *Science*, 369(6500):208–211, 2020.
- [53] Jonathan E Millar, Reinhard Busse, John F Fraser, Christian Karagiannidis, and Daniel F McAuley. Apples and oranges: international comparisons of COVID-19 observational studies in ICUs. *The Lancet Respiratory Medicine*, 8(10):952–953, 2020.
- [54] Xi He, Eric H Y Lau, Peng Wu, Xilong Deng, Jian Wang, Xinxin Hao, Yiu Chung Lau, Jessica Y Wong, Yujuan Guan, Xinghua Tan, et al. Temporal dynamics in viral shedding and transmissibility of COVID-19 . *Nature Medicine*, pages 1–4, 2020.
- [55] Feng Pan, Tianhe Ye, Peng Sun, Shan Gui, Bo Liang, Lingli Li, Dandan Zheng, Jiazheng Wang, Richard L Hesketh, Lian Yang, et al. Time course of lung changes on chest CT during recovery from 2019 novel coronavirus (COVID-19) pneumonia. *Radiology*, page 200370, 2020.

- [56] Yun Ling, Shui-Bao Xu, Yi-Xiao Lin, Di Tian, Zhao-Qin Zhu, Fa-Hui Dai, Fan Wu, Zhi-Gang Song, Wei Huang, Jun Chen, et al. Persistence and clearance of viral RNA in 2019 novel coronavirus disease rehabilitation patients. *Chinese medical journal*, 2020.
- [57] Elisabeth Mahase. Covid-19: Where are we on vaccines and variants? *BMJ*, 372:n597, 2021.
- [58] Jamie Lopez Bernal, Nick Andrews, Charlotte Gower, Chris Robertson, Julia Stowe, Elise Tessier, Ruth Simmons, Simon Cottrell, Richard Roberts, Mark O’Doherty, et al. Effectiveness of the pfizer-biontech and oxford-astrazeneca vaccines on covid-19 related symptoms, hospital admissions, and mortality in older adults in england: test negative case-control study. *bmj*, 373, 2021.
- [59] Eric J Haas, Frederick J Angulo, John M McLaughlin, Emilia Anis, Shepherd R Singer, and Farid Khan et al. Impact and effectiveness of mrna bnt162b2 vaccine against sars-cov-2 infections and covid-19 cases, hospitalisations, and deaths following a nationwide vaccination campaign in israel: an observational study using national surveillance data. *The Lancet*, 397(10287):1819–1829, 2021.
- [60] Emma Pritchard, Philippa Matthews, Nicole Stoesser, et al. Impact of vaccination on new sars-cov-2 infections in the united kingdom. *Nature Medicine*, pages 1546–170X, 2021.
- [61] Mark G Thompson, Jefferey L Burgess, Allison L Naleway, Harmony L Tyner, Sarang K Yoon, Jennifer Meece, Lauren EW Olsho, Alberto J Caban-Martinez, Ashley Fowlkes, Karen Lutrick, et al. Interim estimates of vaccine effectiveness of bnt162b2 and mrna-1273 covid-19 vaccines in preventing sars-cov-2 infection among health care personnel, first responders, and other essential and frontline workers—eight us locations, december 2020–march 2021. *Morbidity and Mortality Weekly Report*, 70(13):495, 2021.
- [62] Matthias an der Heiden and Osamah Hamouda. Schätzung der aktuellen Entwicklung der SARS-CoV-2-Epidemie in Deutschland – Nowcasting. *Epidemiologisches Bulletin*, 2020(17):10–15, 2020.
- [63] Stephen A Lauer, Kyra H Grantz, Qifang Bi, Forrest K Jones, Qulu Zheng, Hannah R Meredith, Andrew S Azman, Nicholas G Reich, and Justin Lessler. The incubation period of coronavirus disease 2019 (COVID-19) from publicly reported confirmed cases: estimation and application. *Annals of internal medicine*, 2020.
- [64] Bundesministerium für Gesundheit. BAnz, Verordnung zum Anspruch auf Schutzimpfung gegen das Coronavirus SARS-CoV-2 (Coronavirus-Impfverordnung – CoronaImpfV), 2021.
- [65] Robert-Koch-Institut. Mitteilung der Ständigen Impfkommision am Robert-Koch-Institut. Beschluss der STIKO zur 2. Aktualisierung der COVID-19-Impfempfehlung und die dazugehörige wissenschaftliche Begründung. https://www.rki.de/DE/Content/Infekt/EpidBull/Archiv/2021/Ausgaben/05_21.pdf, 2021.
- [66] Yinon M Bar-On, Avi Flamholz, Rob Phillips, and Ron Milo. Science forum: SARS-CoV-2 (COVID-19) by the numbers. *Elife*, 9:e57309, 2020.
- [67] Ruiyun Li, Sen Pei, Bin Chen, Yimeng Song, Tao Zhang, Wan Yang, and Jeffrey Shaman. Substantial undocumented infection facilitates the rapid dissemination of novel coronavirus (SARS-CoV-2). *Science*, 368(6490):489–493, 2020.
- [68] Matthias Linden, Sebastian B. Mohr, Jonas Dehning, Jan Mohring, Michael Meyer-Hermann, Iris Pigeot, Anita Schöbel, and Viola Priesemann. Case numbers beyond contact tracing capacity are endangering the containment of COVID-19 . *Dtsch Arztebl International*, 117(46):790–791, 2020.

Supplementary information

S1 Further parameters

Table S1: Parameters for the three main different vaccine uptake scenarios for Finland. Uptakes and averages are to be understood across the eligible (16+) population. For German data see Table 2 in the main text. Italian and Czech data are to be found in Supplementary Information Table S2 and Table S3 respectively.

Group ID	age group	eligible fraction	minimal uptake u_i	mid uptake u_i (default)	maximal uptake u_i	population fraction [28] M_i/M
1	0-19	0.2 (16+)	0.60	0.74	0.88	0.22
2	20-39	1.0	0.65	0.77	0.89	0.25
3	40-59	1.0	0.70	0.80	0.90	0.29
4	60-69	1.0	0.75	0.83	0.91	0.11
5	70-79	1.0	0.80	0.86	0.92	0.07
6	>80	1.0	0.85	0.89	0.93	0.04
average			0.70	0.80	0.90	

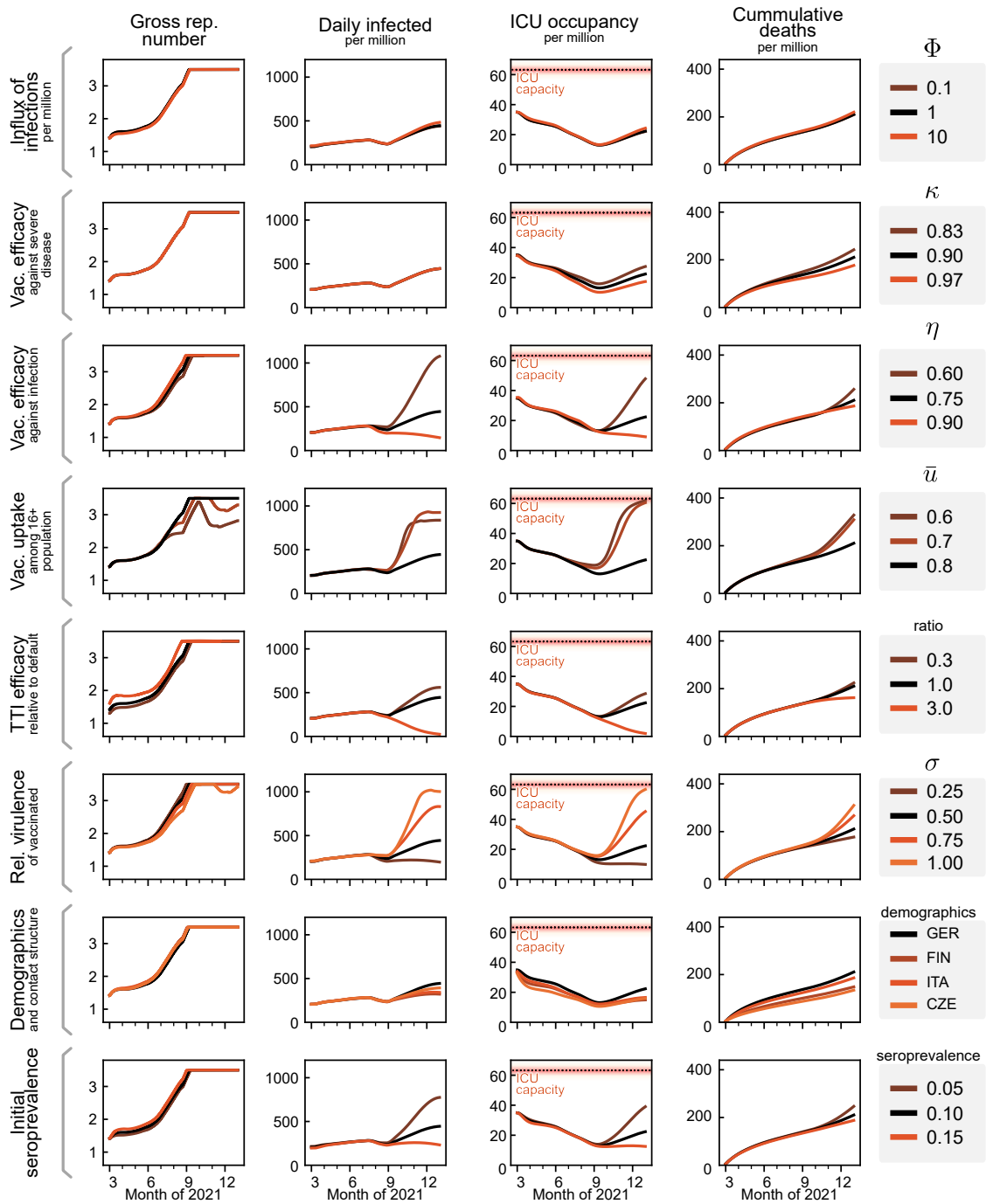
Table S2: Parameters for the three main different vaccine uptake scenarios for Italy. The averages are to be understood across the eligible (16+) population. For German data see Table 2 in the main text. Finnish and Czech data are to be found in Supplementary Information Table S1 and Table S3 respectively.

Group ID	age group	eligible fraction	minimal uptake u_i	mid uptake u_i (default)	maximal uptake u_i	population fraction [28] M_i/M
1	0-19	0.2 (16+)	0.59	0.74	0.88	0.20
2	20-39	1.0	0.64	0.77	0.89	0.28
3	40-59	1.0	0.69	0.80	0.90	0.28
4	60-69	1.0	0.75	0.83	0.91	0.11
5	70-79	1.0	0.80	0.86	0.92	0.09
6	>80	1.0	0.85	0.89	0.93	0.05
average			0.70	0.80	0.90	

Table S3: Parameters for the three main different vaccine uptake scenarios for Finland. The averages are to be understood across the eligible (16+) population. For German data see Table 2 in the main text. Finnish and Italian data are to be found in Supplementary Information Table S3 and Table S2 respectively.

Group ID	age group	eligible fraction	minimal uptake u_i	mid uptake u_i (default)	maximal uptake u_i	population fraction [28] M_i/M
1	0-19	0.2 (16+)	0.60	0.74	0.88	0.23
2	20-39	1.0	0.65	0.77	0.89	0.29
3	40-59	1.0	0.70	0.80	0.90	0.27
4	60-69	1.0	0.75	0.83	0.91	0.11
5	70-79	1.0	0.80	0.86	0.92	0.07
6	>80	1.0	0.85	0.89	0.93	0.03
average			0.70	0.80	0.90	

S2 Sensitivity analysis



Supplementary Figure S1: **Sensitivity analysis centered at default parameters (solid black lines), for the fourth scenario from the main text.** We vary central parameters of the model individually, while keeping all others at their respective default value. For assessing the sensitivity to the TTI efficacy we scale all the capacity limits N_{TTI} , $N_{\text{test}(\text{eff})}$, $N_{\text{test}(\text{ineff})}$ and $N_{\text{no test}}$ (see Methods) by a common ratio.

S3 Eigenvalues of the homogeneous contact matrix

Here we will demonstrate a general case for the eigenvalues of a homogeneous contact matrix, for which every column accounts for the fraction age-groups represent respect to the total population.

Theorem S3.1. *Let C be a square $n \times n$ matrix, such that all columns are identical, i.e., $C_{i,\bullet} = f_i$, $f \in \mathbb{R}^n$, and $\sum_i f_i \neq 0$. Then C is diagonalizable and has a single non-zero eigenvalue $\lambda = \sum_i f_i$.*

Proof. First, we note that the dimension of the kernel of $T : \mathbb{R}^n \rightarrow \mathbb{R}^n$, $T(u) = Cu$, i.e, the vector space $\ker(T) = \{u | Cu = 0\}$ is $n - 1$. Thus, there are $n - 1$ linearly independent vectors associated to the eigenvalue $\lambda = 0$, which algebraic multiplicity has therefore to be equal or larger than $n - 1$. Then, we study the nature of the characteristic polynomial:

$$\begin{aligned}
 p(\lambda) &= \det(C - \lambda I) & (1) \\
 &= \begin{vmatrix} f_1 - \lambda & f_1 & \dots & f_1 \\ f_2 & f_2 - \lambda & \dots & f_2 \\ \vdots & \vdots & \ddots & \vdots \\ f_n & f_n & \dots & f_n - \lambda \end{vmatrix} & (2) \\
 \xrightarrow{\text{column } j - \text{column } 1, \forall j > 1} &= \begin{vmatrix} f_1 - \lambda & \lambda & \lambda & \dots & \lambda \\ f_2 & -\lambda & 0 & \dots & 0 \\ f_3 & 0 & -\lambda & \dots & 0 \\ \vdots & \vdots & \vdots & \ddots & \vdots \\ f_n & 0 & 0 & \dots & -\lambda \end{vmatrix} & (3) \\
 \xrightarrow{\text{row } 1 + \text{row } j, \forall j > 1} &= \begin{vmatrix} \sum_i f_i - \lambda & 0 & 0 & 0 & 0 \\ f_2 & -\lambda & 0 & \dots & 0 \\ f_3 & 0 & -\lambda & \dots & 0 \\ \vdots & \vdots & \vdots & \ddots & \vdots \\ f_n & 0 & 0 & \dots & -\lambda \end{vmatrix} & (4)
 \end{aligned}$$

The highlighted zone in the determinant corresponds to $-\lambda I_{n-1}$, with I_{n-1} the identity matrix in $\mathbb{R}^{n-1 \times n-1}$. Let \tilde{I}_{n-1}^j be I_{n-1} , but with the j 'th row replaced by a row of zeros. Using that $|aA| = a^n |A|$ for an $n \times n$ arbitrary matrix, and that $|D| = \prod d_{ii}$ for a diagonal matrix, we calculate $p(\lambda)$ by minor determinants:

$$p(\lambda) = \left(\sum_i f_i - \lambda \right) |-\lambda I_{n-1}| + \sum_{i=2}^n (-1)^{i-1} f_i \left| \tilde{I}_{n-1}^i \right| \quad (5)$$

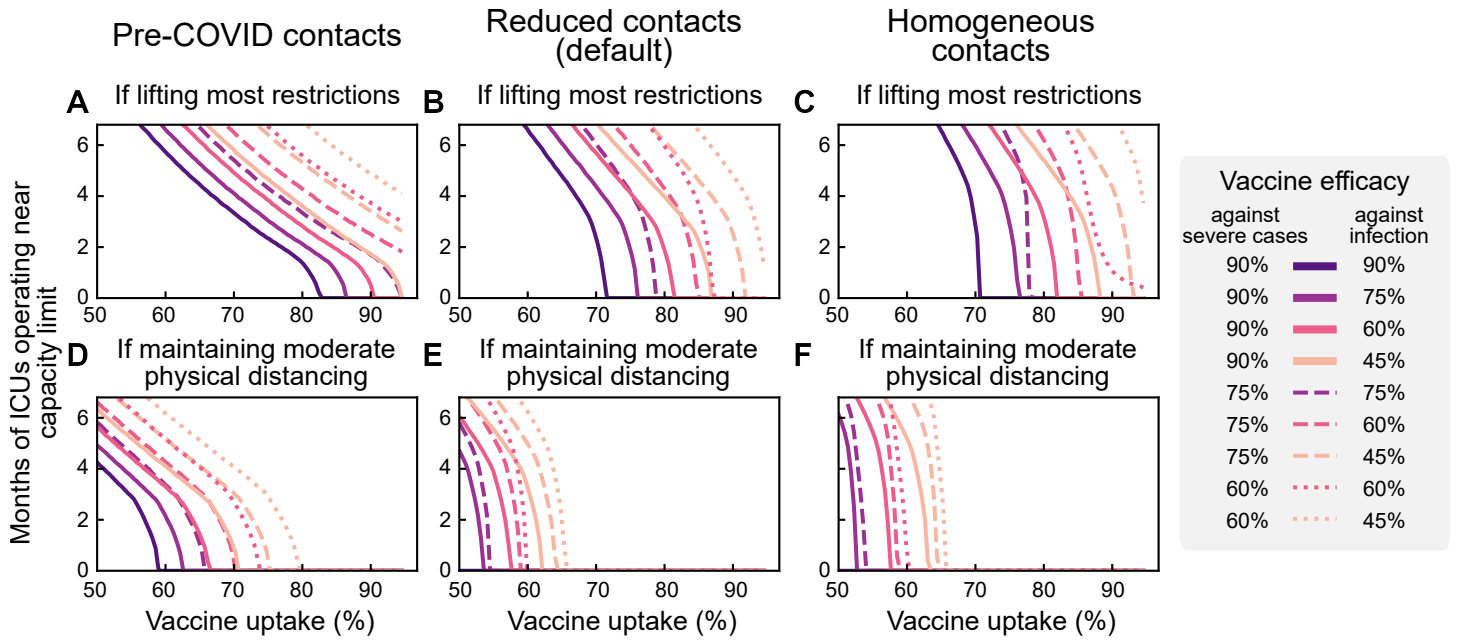
$$= \left(\sum_i f_i - \lambda \right) (-1)^{n-1} \lambda^{n-1}. \quad (6)$$

As we found the last eigenvalue, and, by definition, it has at least one eigenvector, we completed the required set of n eigenvectors and concluded the demonstration. \square

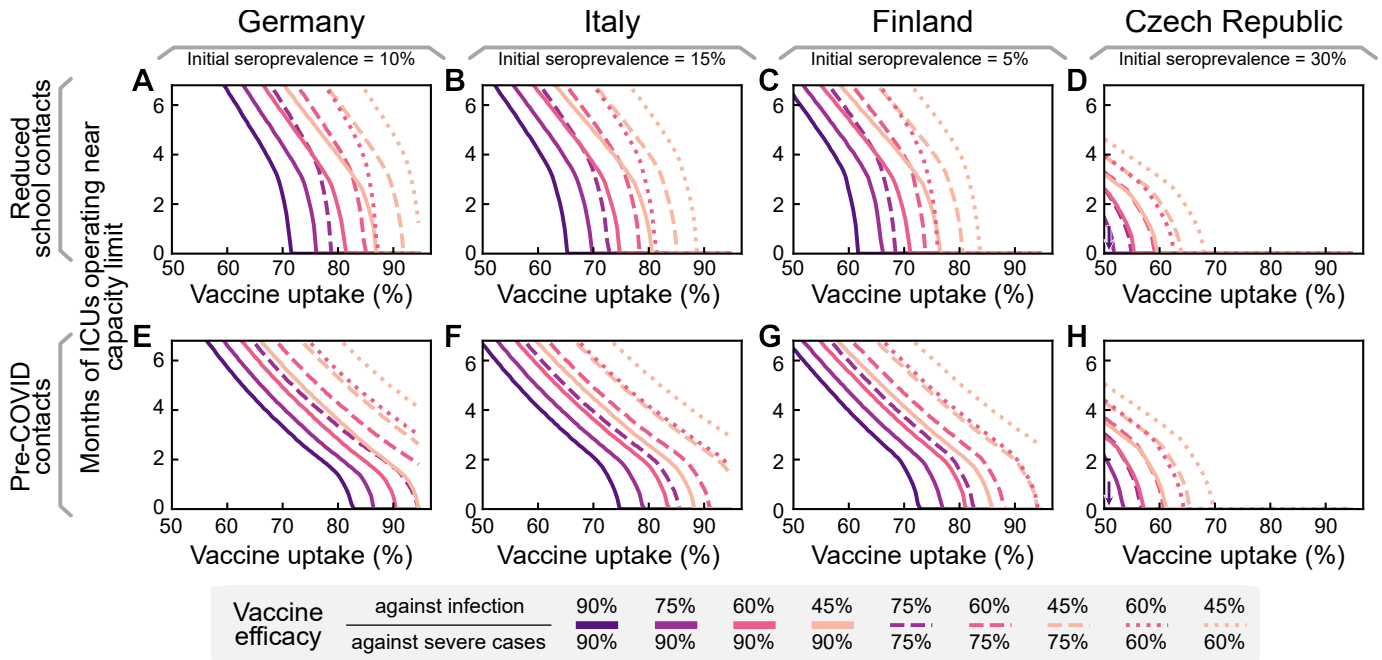
Corollary S3.1.1. *When C is a contact matrix as defined in theorem S3.1 and f accounts for the fraction age-groups represent respect to the total population, the largest eigenvalue of matrix C is 1.*

Proof. Direct from theorem S3.1, knowing that $\sum_i f_i = 1$. \square

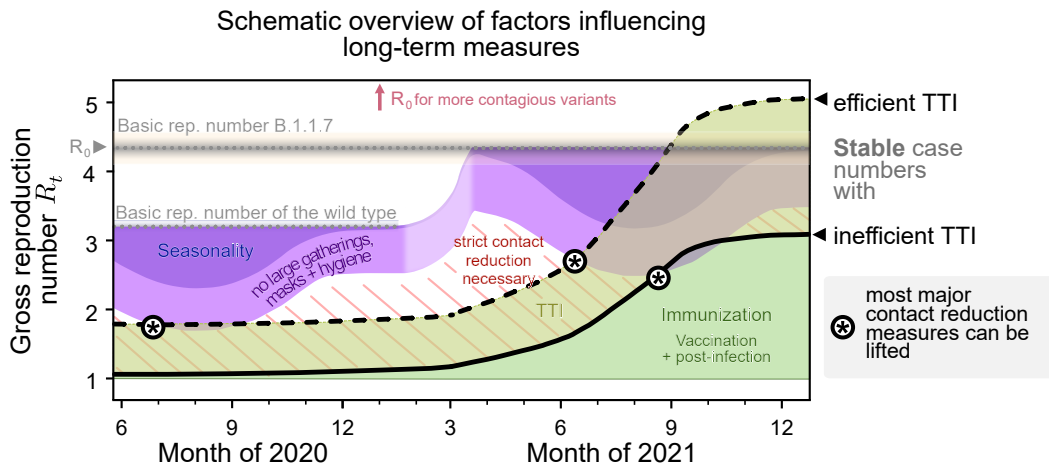
S4 Additional figures referenced in the main text



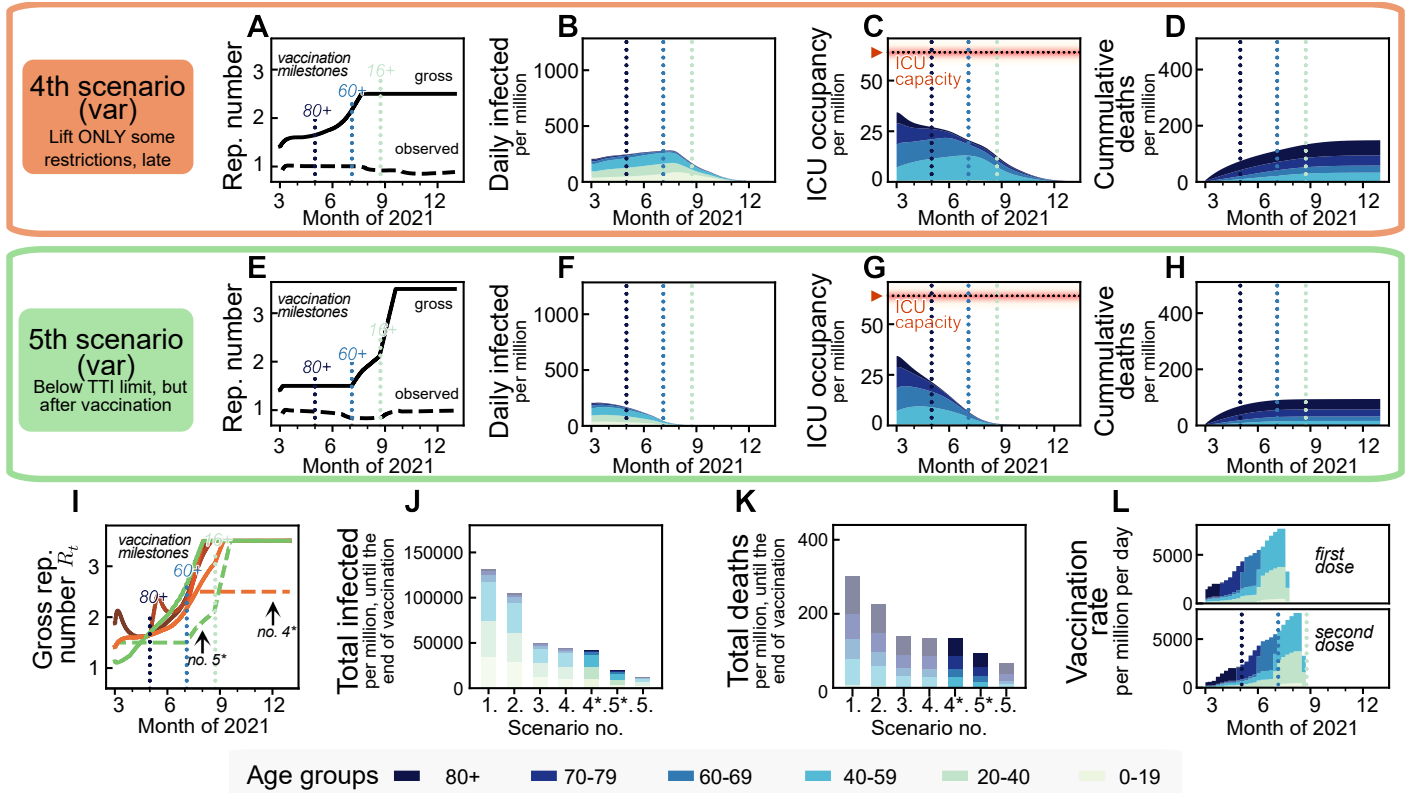
Supplementary Figure S2: **Contact structure can have a significant impact on the population immunity threshold.** We assume that infections are kept stable at 250 daily infections until all age groups have been vaccinated. Then most restrictions are lifted, leading to a wave if vaccine uptake has not been high enough (see Fig. 4 A). We measure the severity of the wave (quantified by the duration of full ICUs) for varying uptake and vaccine efficacies for different contact structures (see Fig. 7 A,B,C). **A-C:** The duration of the wave (measured by the duration of full ICUs) depends on the vaccine uptake and on the effectiveness of the vaccine measured by its efficacy at preventing infection (shades of purple) and severe illness (vaccine efficacy, full vs dashed vs dotted). **D-F:** If some NPIs are kept in place (such that the gross reproduction number goes up to $R_t = 2.5$), ICUs would be prevented from overflowing even in some cases of lower vaccine effectiveness. If precautionary measures are dropped in all age groups, including schools (A,D) the required uptake to prevent a further severe wave is increased by about 10% when compared to our default scenario of some continued measures to reduce the potential contagious contacts in school settings (B,E) or to completely homogeneous contacts (C,F). Not all combinations of vaccine effectiveness are possible as the vaccine efficacy against severe illness is by definition larger as the protection against any infection at all.



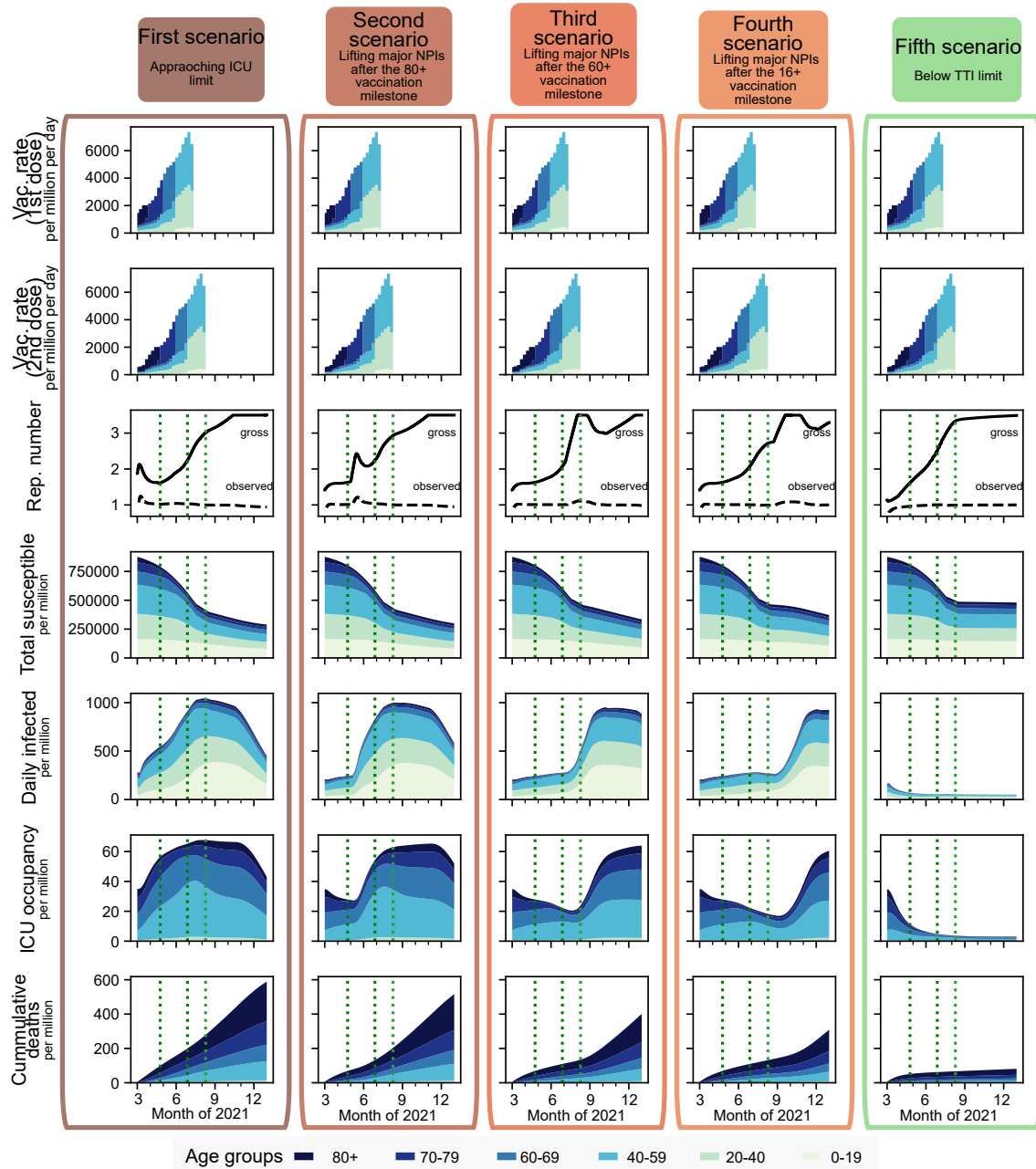
Supplementary Figure S3: **EU countries with different demographics have very similar dynamics – but the required vaccine uptake to guard against further severe waves is most sensitive to the initial seroprevalence.** Extended version of Fig. 5, including more combinations of vaccine efficacies. **A–D:** If releasing all measures to pre-COVID contacts, keeping only some measures aiming to cup the reproduction number at 3.5. **E–H:** If releasing all measures to pre-COVID contacts, keeping only some measures aiming to cup the reproduction number at 3.5 and halving the contagiousness of contacts at school ages.



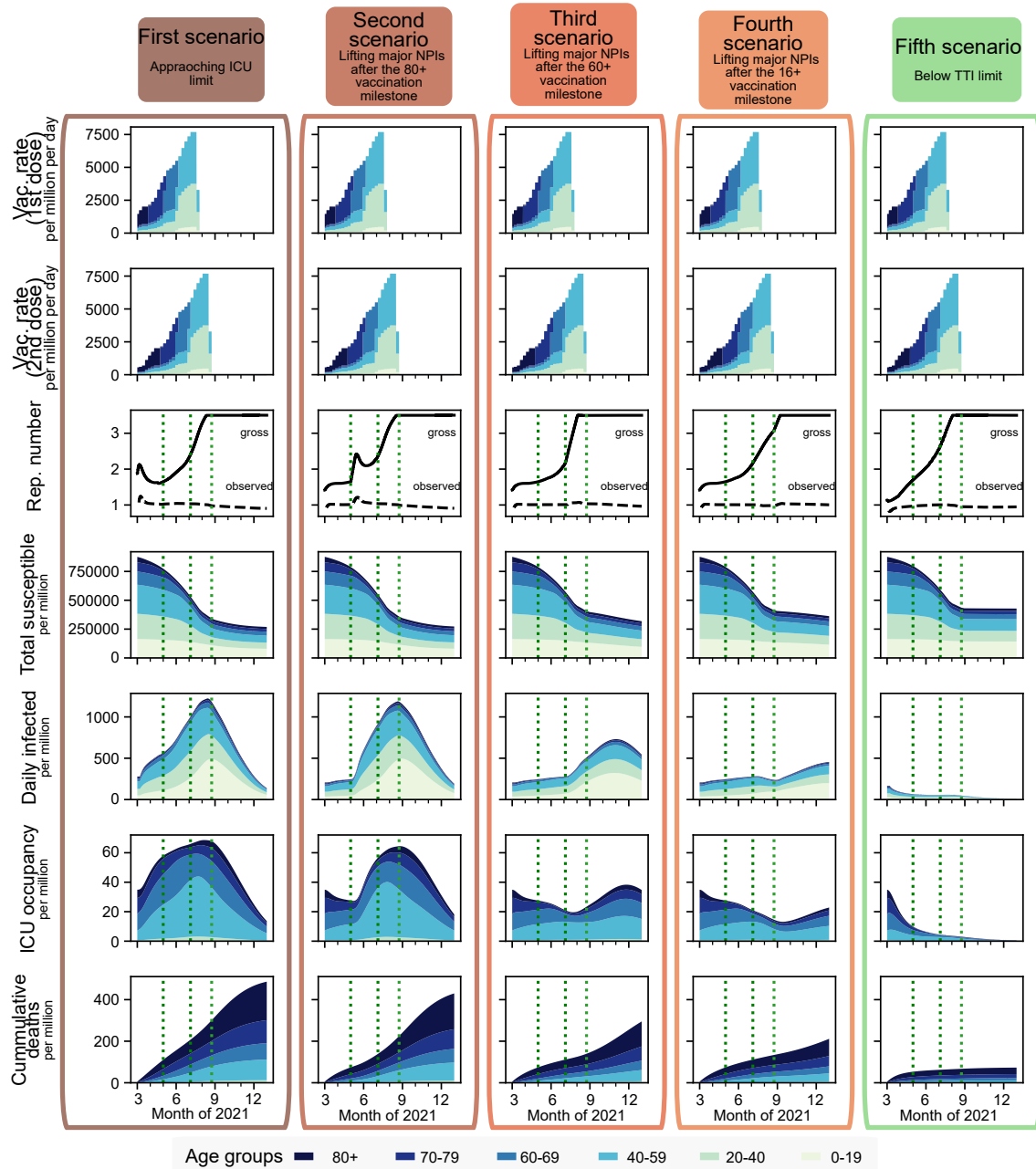
Supplementary Figure S4: **Even with the emergence of the highly contagious B.1.1.7 variant vaccinations are a promising mid-term strategy against COVID-19. Staying at low case numbers can greatly increase the individual freedom, especially in the long-term.** Schematic outlook into the effects of vaccination and the B.1.1.7 variant of SARS-CoV-2 on the societal freedom in the EU in 2021 compared to 2020 (see also the caption for Fig. 1 A). In 2020, seasonality effects and efficient test-trace-and-isolate (TTI) programs at low case numbers allowed for stable case numbers with only mild restrictions during summer, until about September. In 2021, vaccinations are expected to allow for greater freedom, but also a more contagious variant (B.1.1.7) is prevalent across the EU. Efficient TTI at low case numbers would thus help lifting major restrictions earlier. The exact transition period between the wild type and B.1.1.7 (light purple shaded area) varies regionally.



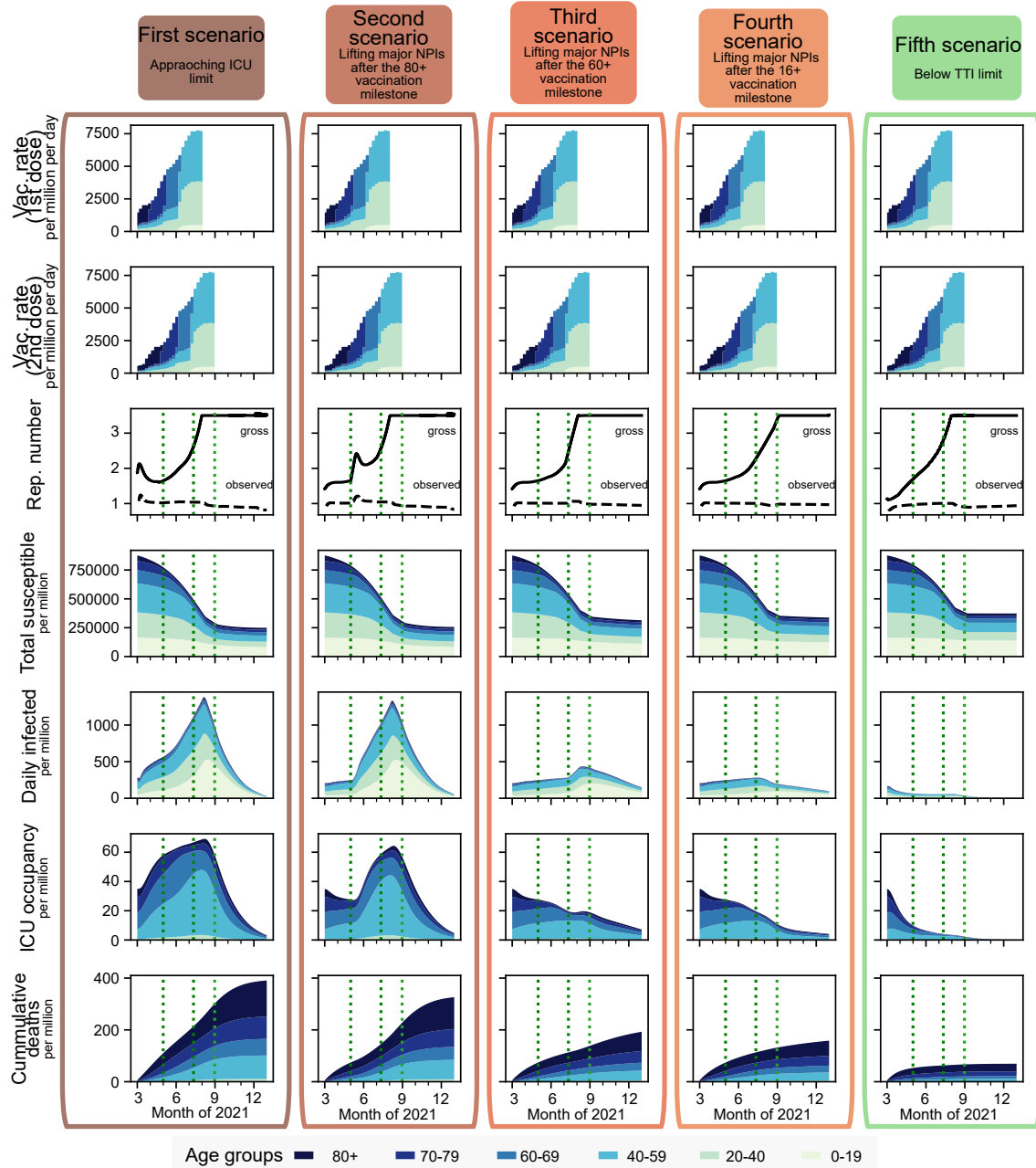
Supplementary Figure S5: **Lowering the case numbers without the most stringent restrictions opens a middle ground between freedom and fatalities and prevents a new wave in the long term.** **A–D:** Variation of the fourth scenario from the main text (see Fig.3), where moderate restrictions are kept in place in the long term (letting the gross reproduction number go up to 2.5, compared to 3.5 in the default scenarios). **E–H:** Variation of the fifth scenario from the main text (see Fig.2) avoiding the strict initial restrictions. Keeping the gross reproduction number at a moderate level (1.5) until the everyone above 60 has been offered vaccination allows to decrease case numbers steadily. Over the summer a slight gradual increase in the contacts is allowed and all NPIs expect for test-trace-and-isolate (TTI) and enhanced hygiene are lifted when everyone received the vaccination offer (increasing the gross reproduction number to 3.5). **I:** The variation of the fourth scenario initially allows for the same increase in freedom as all the main scenarios, but needs more restrictions in the long term. The variation of the fifth scenario calls for stricter NPIs in the mid-term, but grants high freedom after summer. **J,K:** Both proposals lead to low number of infections and fatalities. **L:** Projected vaccination rates (see Fig. 2).



Supplementary Figure S6: **Long-term control strategies** from main text figures 2 and 3. Scenarios using default protection against infection $\eta = 0.75$ and **low vaccine uptake of 70%** among the adult population.

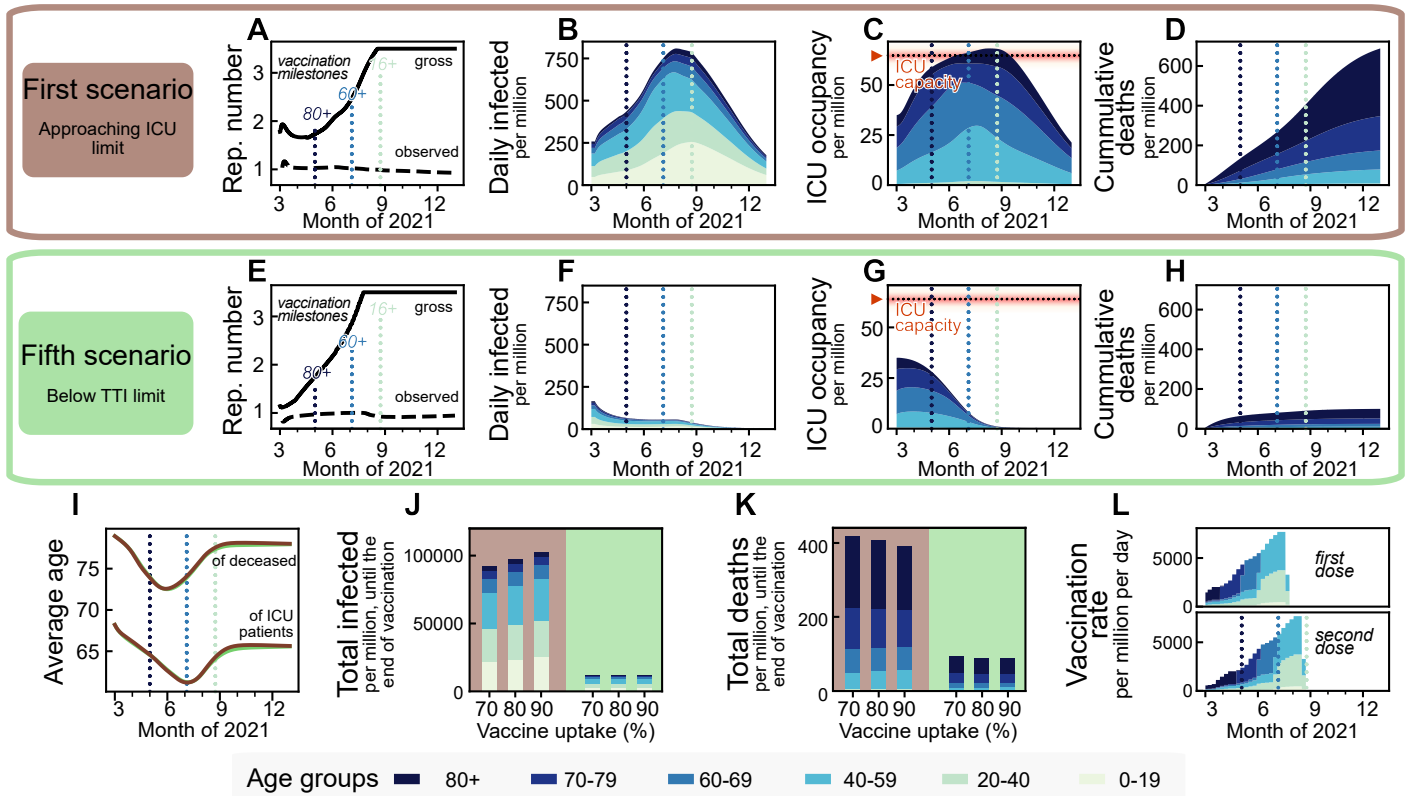


Supplementary Figure S7: **Long-term control strategies** from main text figures 2 and 3. Scenarios using default protection against infection $\eta = 0.75$ and **default vaccine uptake of 80%** among the adult population.

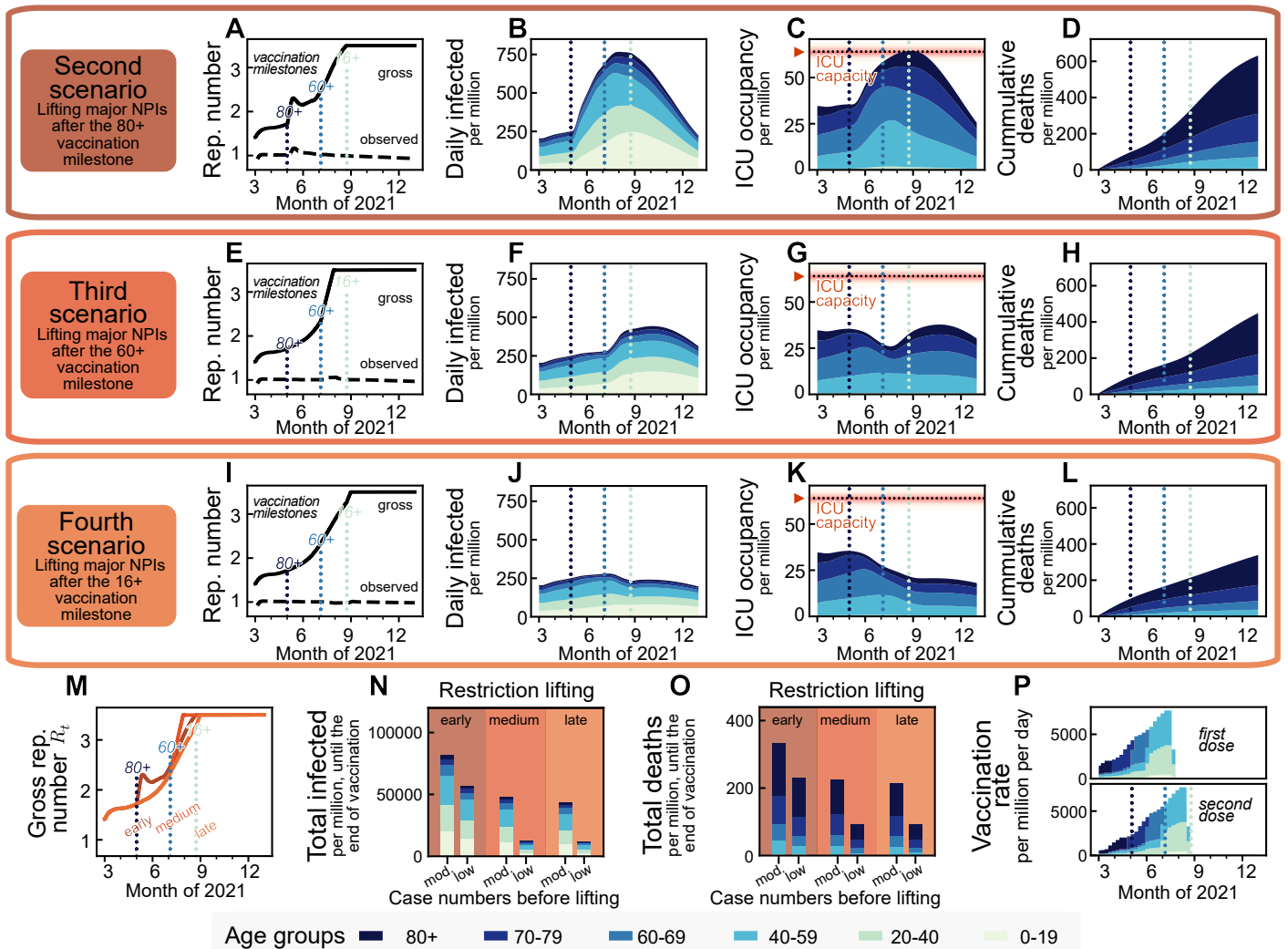


Supplementary Figure S8: **Long-term control strategies** from main text figures 2 and 3. Scenarios using default protection against infection $\eta = 0.75$ and **high vaccine uptake of 90%** among the adult population.

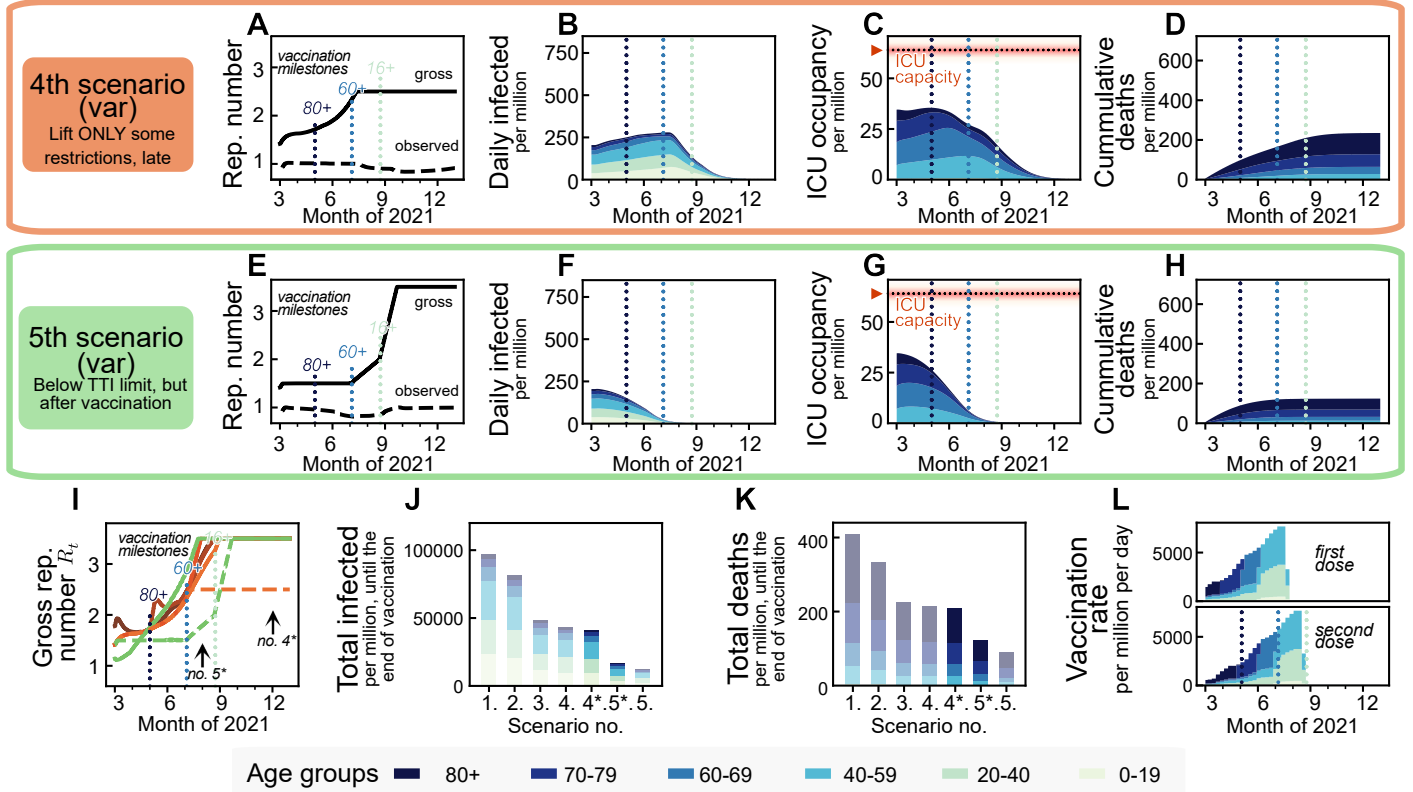
S5 Mirror figures using different contact matrices



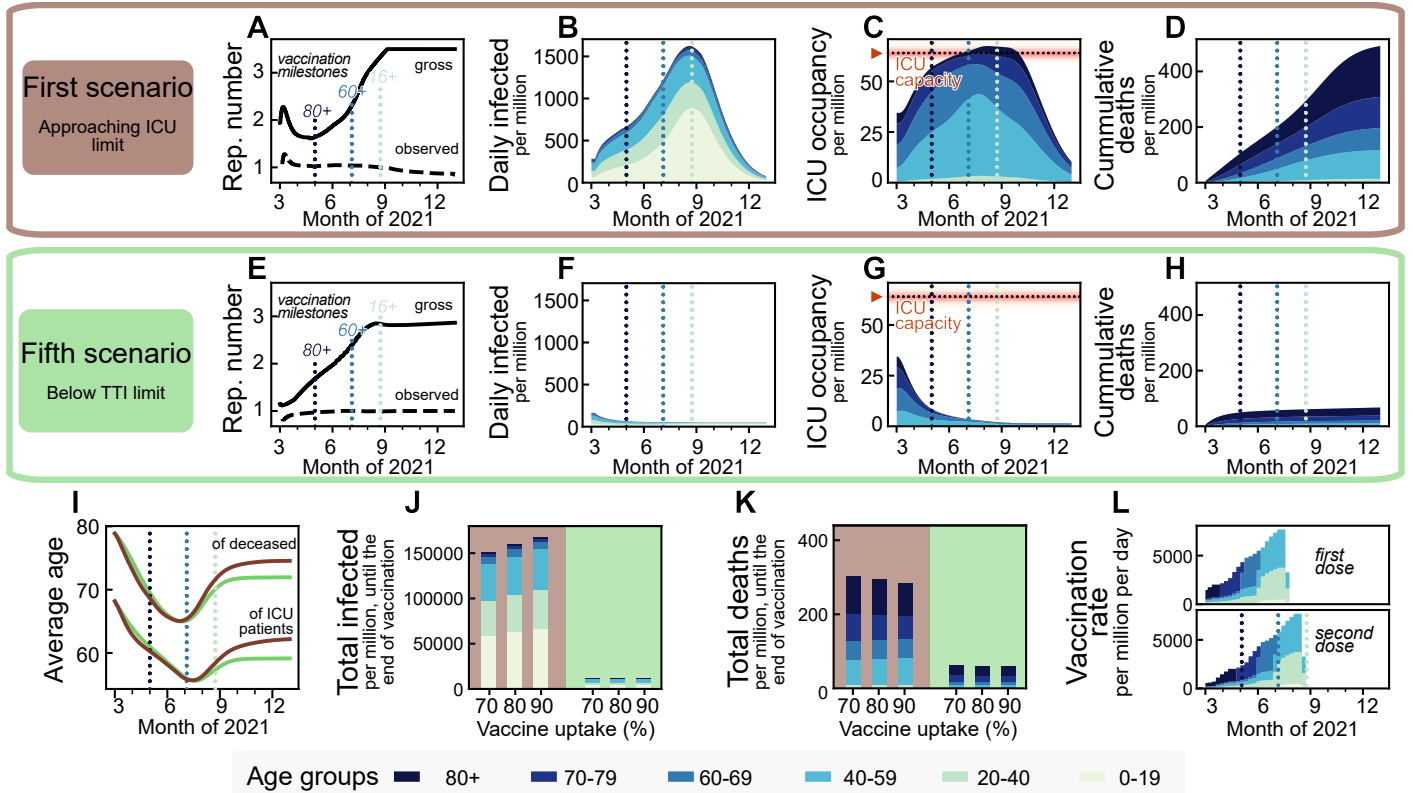
Supplementary Figure S9: Mirror of Fig. 2, using a homogeneous contact structure (see Fig. 7 A).



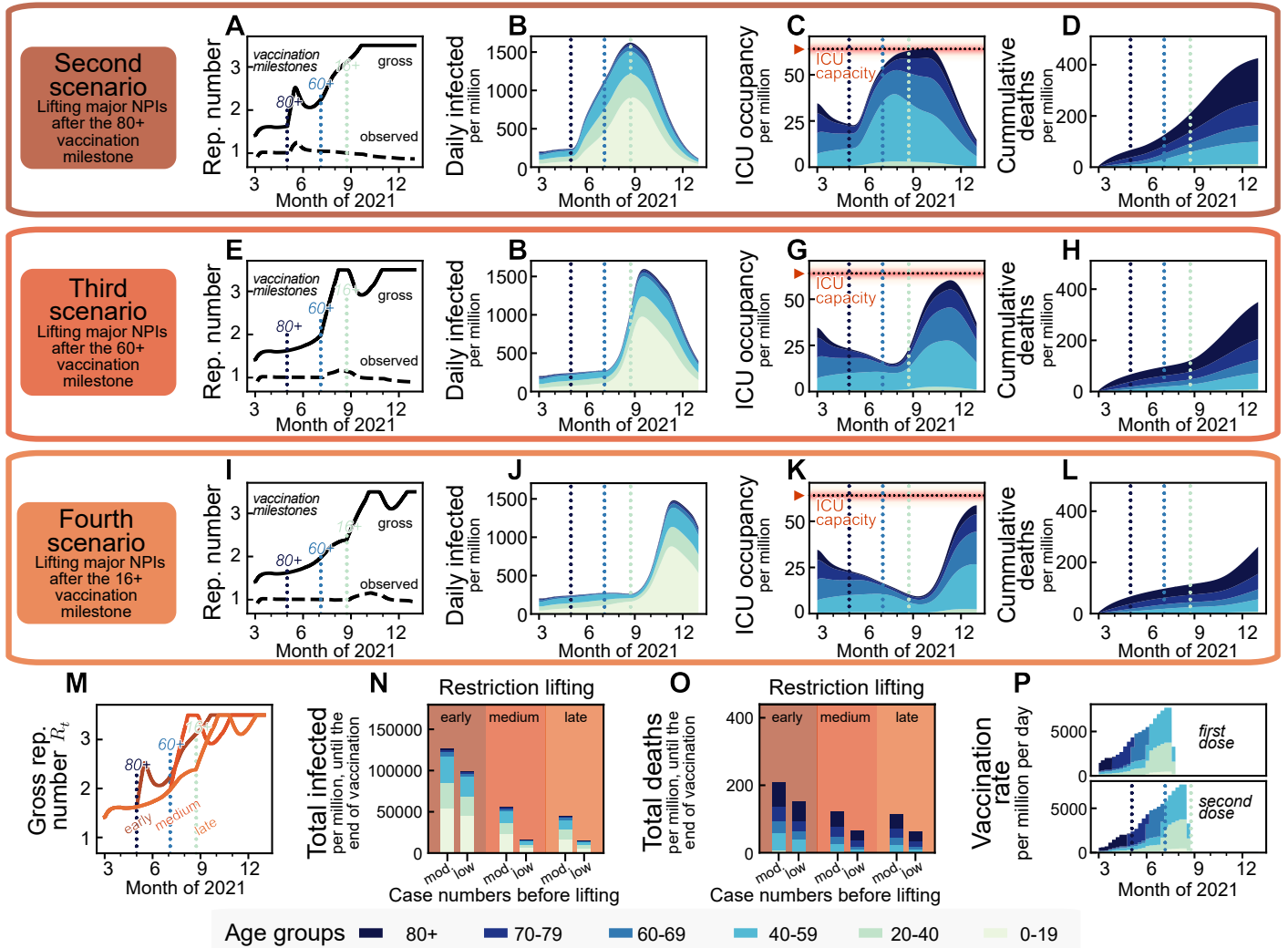
Supplementary Figure S10: Mirror of Fig. 3, using a homogeneous contact structure (see Fig. 7 A).



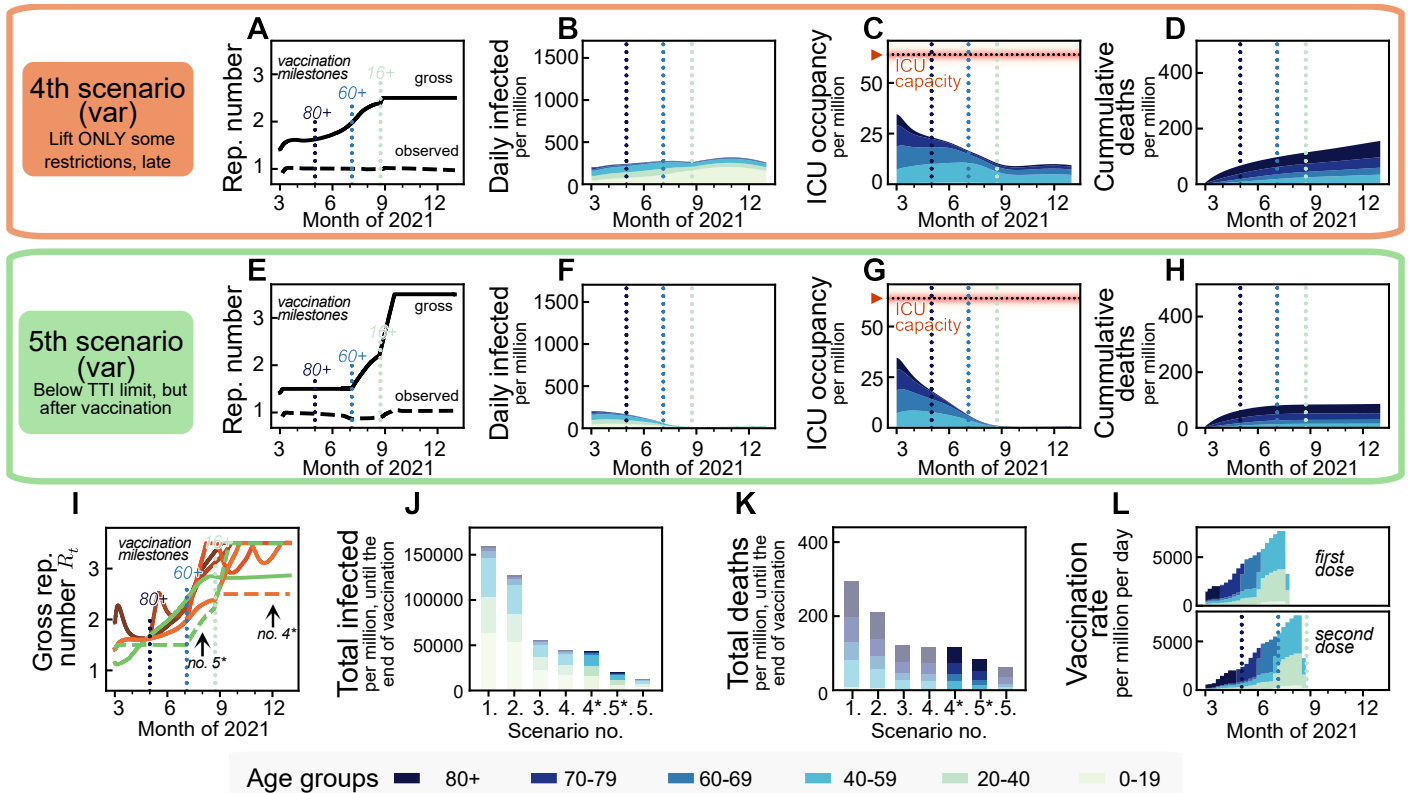
Supplementary Figure S11: Mirror of Figure S5, using a homogeneous contact structure (see Fig. 7 A).



Supplementary Figure S12: Mirror of Fig. 2, using an empirical pre-COVID contact structure (see Fig. 7 B).



Supplementary Figure S13: Mirror of Fig. 3, using an empirical pre-COVID contact structure (see Fig. 7 B).



Supplementary Figure S14: Mirror of Figure S5, using an empirical pre-COVID contact structure (see Fig. 7 B).